Field-derived phosphorus accumulation rates and fractionation in bioretention cells

by

Ariel Lisogorsky

A thesis

presented to the University of Waterloo

thesis requirement for the degree of

Master of Science

in

Earth Sciences (Water)

Waterloo, Ontario, Canada, 2022

Author's Declaration

This thesis consists of material all of which I authored or co-authored: see Statement of Contributions included in the thesis. This is a true copy of the thesis, including any required final revisions, as accepted by my examiners.

I understand that my thesis may be made electronically available to the public.

Statement of Contributions

This thesis originates from a draft consists of a co-authored, manuscript-format paper. As first author I coordinated and performed majority of the laboratory and data analyses presented. I also drafted and edited the manuscript and wrote the code for data collation, analysis and visualizations/figures shown within it. The contributions of the listed co-authors are as follows: Dr. Fereidoun Rezanezhad and Dr. Elodie Passeport advised and provided direction on the data analysis, interpretation, and presentation in the manuscript. Both also significantly contributed to manuscript structure and style decisions. Dr. Philippe van Capellen and Dr. Chris Parsons also provided advice on study design and data interpretation. Dr. Mahyar Shaffi Hasabanadi and Dr. Fereidoun Rezanezhad oversaw initial field site selection and sample collection.

Though I performed the plurality of the preparation and chemical analysis of the samples for which data is presented, various members of the Ecohydrology Research Group performed sections of the analytical procedures. Marianne VanderGriendt and Shuhuan Li, assisted me with various tasks throughout the analytical process for my samples as well as initial training on new methods.

Stephanie Slowinski, Yubraj Bhusal, Bowen Zhou, Jovana Radosavljevic, Alina Arvisais and I were all part of the team that performed the sequential (SEDEX) extractions of the samples presented in the manuscript.

Data for historical measurements taken at the field site were extracted from a technical report initially published by the Credit Valley Conservation Authority,

Abstract

Bioretention cells are commonly used green infrastructure in urban stormwater management systems. They show promising performance in managing stormwater and mitigating a multitude of pollutants. In urban catchments, they have been shown to favorably reduce the 'flashiness' and overall volume of surface flow resulting from storm events by promotion of storage, groundwater infiltration, and evapotranspiration. Previous studies have shown highly variable phosphorus (P) removal impacts for bioretention cells, establishing a need for more comprehensive understanding of P biogeochemistry within bioretention systems to identify the processes that are responsible. In this study, a sequential extraction (SEDEX) method was used to analyze concentrations of six P fractions in filtration media samples collected from a set of 12-year-old interconnected bioretention cells in Mississauga, Ontario, Canada. The newly acquired data, when combined with previously available data for the site, showed an average total P (TP) accumulation rate of 66-78 mgP kg^{-1} y^{-1} in the top 10 cm of media and 4-32 mgP kg^{-1} y^{-1} in the 25cm – 45cm deep region. Analysis of the measured concentrations using non-metric dimensional scaling (NMDS) identified that variable clusters associated with redox-sensitive P and organic matter-associated P (organic, humic-bound P, and exchangeable) fractions best represented TP variation in the system. In contrast, little of the overall TP variation in the media was explained by the Ca or calcium-associated P concentrations. Evidence of continued P accumulation with a preferential near-surface enrichment in the system suggests that bioretention cells have potential for long-term P capture, especially if coupled with targeted media replacement of the surface media. Additionally, the difference between calcium and redox sensitive fractions suggests that further consideration of the redox sensitivity of aged cells should be considered in their design. Finally, this difference highlights the need to employ methodologies that distinguish redox- and calcium- associated

fractions when attempting to speculate about the mechanisms responsible for the P distributions observed within bioretention systems.

Acknowledgements

I cannot thank my supervisors, Dr. Fereidoun Reznezhad and Dr. Elodie Passeport enough for their understanding, guidance and support throughout this process. I want to particularly recognize their continued encouragement and advice that carried me through the seemingly endless stream of challenges I was able to encounter during this project. Keeping me on the right track and working in the right direction is hard, whether with respect to structure, experiment decisions or interpretation. Thank you Fereidoun for continuing to reassure me that this is possible and that I was making progress during my almost constant state of doubt about the fact and providing me the structure to do so. Thank you Elodie for guiding my methods and decisions to sort through and extract meaningful, novel and defensible conclusions from the challenging dataset the "unprecedented circumstances" this pandemic created for the project.

It was also instrumental to have my other two committee members, Dr. Philippe Van Cappellen and Dr. Chris Parsons who shared their incredibly broad knowledge base and almost immediately responded every obscure question I asked of them, usually with a dozen articles of background reading to match. Thank you both for the guidance, insight and support.

I want to acknowledge the rest of my research team in the urban project of the Ecohydrology group for helping me to discuss and develop ideas, joining me on surprise runs to the field and helping with sample analysis. Thank you, Steph, for your support with almost all aspects of this project, whether emotional, technical, social, scientific etc. I cannot overstate how much your contributions improved the content this thesis and my psychological wellbeing while writing it. Thank you to Yuba, Bowen, Jovana, Mahyar & Konrad for your assistance, feedback, discussion and lab support.

Thank you, Marianne and Shuhuan for helping me to learn and refine the laboratory methods I needed. I also want to thank them, Danielle and all the other research assistants who helped analyze and validate results from the absolutely massive number of samples this project needed.

I also acknowledge the funding provided by the Canada Excellence Research Chair (CERC) program in Ecohydrology and the Natural Sciences and Engineering Research Council of Canada (NSERC) Strategic Partnership Grant (STPGP 521515-18. I thank Credit Valley Conservation (CVC) for sharing the data and access to the site where the filtration media samples were collected.

Finally, and on a more personal note, I want to thank a few family and friends who kept me sane under pressure. My parents and sister, for catching me at my lowest, reassuring me all was safe and convincing me it could be done. My amazing partner, Hannah, whose brilliance knows no bound, kindness has no equal in my life, and whose humility would probably prefer I keep this sentence brief. And finally, Riley, Shirley, Nilofar, Emily, Kat and so many other friends, all of whom were always there to lend an ear and often directly or indirectly helped to make sure my basic human needs were met when I forgot to do so. Thank you all.

Dedication

This thesis is dedicated to my grandfather, Ezequiel Allami, who passed away shortly after the start of this journey.

Table of Contents

List of Figures

List of Tables

List of Abbreviations

Al aluminium

Ca calcium

Fe iron

Mg magnesium

Mn manganese

P phosphorus

- **TP** total
  - **TDP** total dissolved
  - **DRP** dissolved reactive
  - **SRP** soluble, reactive. (Comparable to P^{I}_{Ex})
- $\mathbf{P}^{I}_{Ex}$ loosely bound, exchangeable
- $\mathbf{P}^{II}_{Hum}$ humic-bound
- $\mathbf{P}^{III}_{Fe}$ redox-sensitive, Fe-bound
- $\mathbf{P}^{IV}_{Ca}$ authigenic apatite, Ca-bound
- $\mathbf{P}^{V}_{Det}$ detrital apatite, Ca-mineral-bound
- $\mathbf{P}^{VI}_{Org}$ organic-matter-bound

C carbon

- **TC** total
- **TIC** total inorganic
- **TOC** total organic

N Nitrogen

- **TN** total Nitrogen (N)
- **TIN** total inorganic
- **TON** total organic

CVC Credit Valley Conservation Authority

NMDS non-metric dimensional scaling

PCA principal component analysis

1 Introduction

Bioretention cells are common stormwater control systems designed to reduce peaks and volumes of urban stormwater runoff and provide secondary benefits such as urban water quality improvement (CVC and TRCA, 2010; Davis et al., 2009; Spraakman, 2021; Spraakman et al., 2020). They consist of a depression in the ground where the natural soil has been replaced by an engineered, usually sand-based media, covered with mulch and planted with a variety of vegetation. While they are consistently efficient at reducing concentrations and loads of particulate pollutants such as suspended solids and microplastics (Smyth et al., 2021; Spraakman, 2021), they exhibit poorer performance for dissolved pollutants such as phosphorus (P) (Géhéniau et al., 2015; Goor et al., 2021; Li and Davis, 2016a; Manka et al., 2016).

Phosphorus is regulated in many water bodies across the world due to its role in eutrophication in P-limited water bodies. In Canada, for example, though no uniform national water quality criterion exists for P, there are P concentration range targets depending on the water body trophic status (Canadian Council of Ministers of the Environment, 2004). In the United States, recommended total phosphorus (TP) levels are at 0.05 to 0.1 mg L^{-1} for surface water bodies with more granular guidelines at regional levels (US EPA, 2022, 1986). In Europe, while the Water Framework Directive does not specify a unique TP concentration target, maximum allowable TP concentrations range between 0.005 and 0.5 mgP L^{-1} depending on the countries and water bodies (Poikane et al., 2019). It has been reported that the urban stormwater runoff carries both particulate and dissolved P, both containing inorganic and organic fractions of P, with TP concentrations commonly ranging from 0.03 mgP L^{-1} to 0.3 mgP L^{-1} (Brezonik and Stadelmann, 2002; Goor et

al., 2021; Hobbie et al., 2017; Janke et al., 2017; Miguntanna et al., 2013; Song et al., 2015; Song and Song, 2019; Yang and Lusk, 2018).

Phosphorus treatment performance of bioretention systems has been often looked at in a very general manner focusing on either TP or reactive phosphorus fractions without consideration of their specific chemistry and impact. The majority of laboratory experiments (Ding et al., 2019; Hsieh et al., 2007; Spraakman et al., 2020; Yan et al., 2017), databases (like the international Stormwater Best Management Practice database), and models (Summarized in A7) focus primarily on inflow/outflow concentrations of P (as total and/or dissolved) in systems. To elucidate the mechanisms primarily responsible for P capture and better predict removal performance under altered conditions, a improved understanding of the P chemistry in the input load, effluent, and filtration media is necessary. Understanding P loading and fate within bioretention cells is important to predict how their performance will develop over time, as well as how their treatment performance may change under different environmental conditions (McManus and Davis, 2020).

Mechanistic processes like particle capture (Blecken et al., 2010; Ding et al., 2019; Li and Davis, 2008a, 2008b), surface chemistry (Yu et al., 2015; Zhang et al., 2018) and biological processes (Denich et al., 2013; Li et al., 2021) have been assessed at the laboratory and mesocosm scales but have not been validated at the time scale and complex environmental conditions that a bioretention system will experience during its design life. Studies at that scale have been more inconsistent both in practice (Spraakman et al., 2020) and results (Géhéniau et al., 2015; Goor et al., 2021; Komlos and Traver, 2012; Liu et al., 2021; Lucke and Nichols, 2015).

Compared to their target design lifetimes of over 20 years (Johnson and Hunt, 2020), most bioretention cells studied were built in the past 5 years and performance of systems near the end

of their design life has only been reported in a few studies (Johnson and Hunt, 2020, 2019; Marvin et al., 2020; Spraakman et al., 2020; Willard et al., 2017). The lifetime of bioretention cells with respect to P retention was estimated at several decades for various types of amendments. For example, water treatment residues were assessed with 15 year loading equivalents (Zhang et al., 2018), (Marvin et al., 2020). Such estimates, however, were obtained from extrapolations of lab-obtained data, which may not accurately represent realistic field conditions.

Most studies and models that discuss P accumulation rates within cells or their specific components do so based only on input and output loads derived from input volumes and concentrations (Summarized in A7). These estimations often rely on (untested) assumptions about water and P fate within the system and attribute the missing loads to accumulation and removal within the system (Davis, 2008; Goor et al., 2021; Li and Davis, 2016a). Actual field derived data of changes observed in media are rare.

Field conditions are considerably more complex than experimental conditions controlled in the lab due to urban runoff chemistry (pH, redox potential, ion composition, distribution between particulates and dissolved P concentrations), filtration media properties (chemical and physical composition, hydraulic conductivity), and environmental factors (temperature, precipitation depth, intensity and duration, freeze-thaw cycles) that change over time. There is therefore a need to evaluate P reaction mechanisms and estimate P accumulation rates under realistic field conditions. In this study, in addition to a previous dataset from the study site, a sequential extraction (SEDEX) method was used to analyze concentrations of six P fractions in filtration media samples collected from a 12-year-old bioretention system consisting of a sequence of hydraulically connected cells. The main objectives were to 1) provide field-derived estimates of P accumulation rates in a

conventionally-designed bioretention system, and 2) characterize P reaction mechanisms from field-obtained filtration media TP distributions and P fraction concentrations.

2 Materials and Methods

2.1 Bioretention cell site

A 6-cell bioretention system installed and managed by Credit Valley Conservation (CVC) in a residential area of Mississauga, Ontario, Canada was selected for this study (Figure 1). The cells have been operating since 2012 and they receive drainage from a 6,456-m^2 catchment comprising of 1,913 m^2 of residential roads, a permeable pavement sidewalk, and a parking lot (Credit Valley Conservation, 2016). Approximately 49% of the surface area from which the bioretention cell system receives drainage is impervious. The size of each bioretention cell is approximately 14.7 m × 1.6 m and they were initially designed with layers of 5-7 cm deep mulch, 45 cm filtration media (85-88% sand and 8-12% fines with 3-5% organic content by weight), 15 cm sand, and storage regions of varying depths interconnected by a single perforated drainage pipe (Figure 1). The underdrain design hydrologically links the storage regions in the cells in series from the most upstream cell (#1) to the most downstream cell (#6). Notably, the maximum altitude reached by the pipe connecting the lower set of cells (#3 to #6) is within the elevation range of the filtration media in cell #6 (Figure 1b). The bioretention cells are separated from the surrounding soil by a non-woven geotextile. A notched weir and level logger have been used since the installation of the system to monitor the rate of outflow from the bioretention cells to storm sewers at 10-minute intervals during storm events.

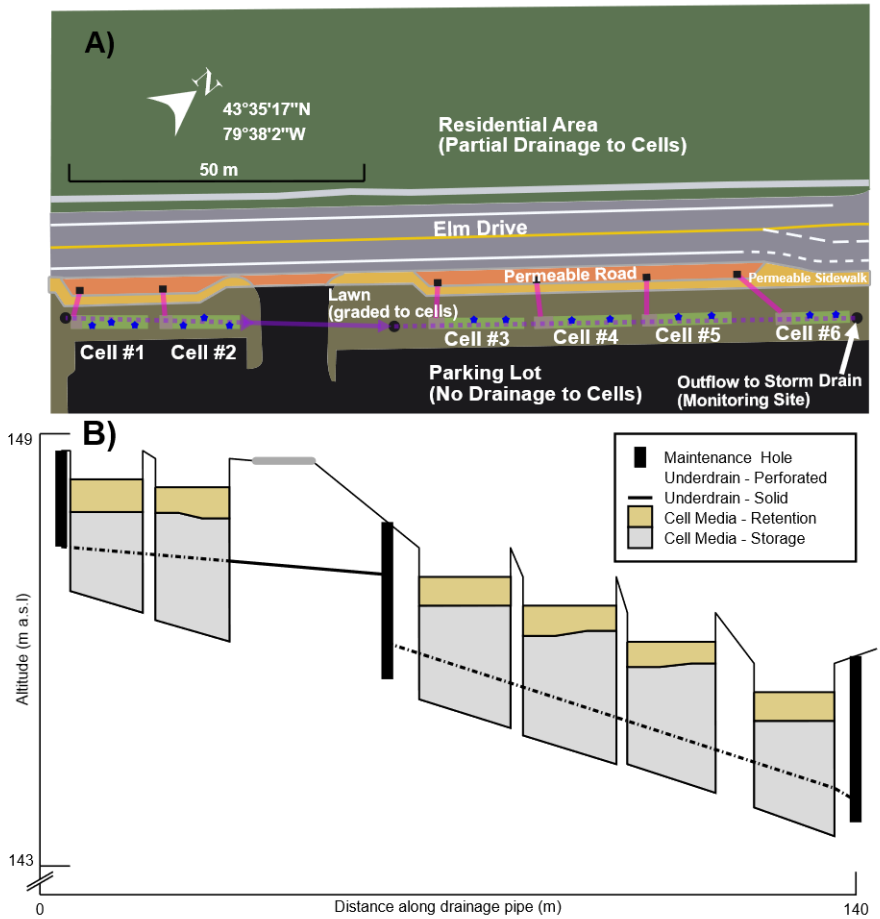

Figure 1: Simplified Elm Drive site schematic showing main surface drainage areas (A) and elevation profile (B). Street grate inlet pipes to cells shown in pink and perforated underdrain shown as a dotted purple line. Approximate locations of the cores taken in 2019 are shown as blue stars. The cells were numbered from upstream to downstream. The elevation profile of the system (B) is shown aligned with the upper diagram illustrating heights of bioretention media (yellow) and water storage, bedding gravel regions (gray), and drainage structures in the system.

2.2 Filtration media sample collection and characterization

Data from analyses of filter media grab samples from 3 different cells (#1, #4, and #6) in years 1, 2 and 4 after construction (*i.e.*, in 2013, 2014, and 2016) and from 2 depths (roughly 0-10 and ~35-45 cm) were obtained from CVC (Credit Valley Conservation, 2016). Additional filtration media samples were collected in November 2019 (7 years post-construction) from all 6 cells using 25-cm long shuttle corers (Pallud and Van Cappellen, 2006), including three cores each from cells #1

and #2 and two cores each from cells #3, #4, #5, and #6 (Figure 1). The filtration media samples were sliced every 2 cm and frozen to -20°C for three days, freeze-dried (Labonco Bulk Tray Dryer Catalog No: 7806021), homogenized, ground with a mortar and pestle, sieved to 125 μm and stored in a desiccator. All freeze-dried and sieved samples were analyzed for TP (see section 2.3). Other analyses were performed on different subsets of the samples (results and coverage presented in A1 and A2). Samples from cell #2 were most frequently used because their cores were the deepest. For the sake of simplicity, the central depth of the slices will be used hereafter when referring to the depths of the individual samples collected (*i.e.* a 3 cm depth represents a slice covering the 2-4 cm depth range).

A subset of samples was analyzed for P fractions using a sequential extraction (SEDEX) method (see Section 2.4) (Baldwin, 1996; Ruttenberg, 1992; Ruttenberg et al., 2009). Another subset was analyzed for total carbon (TC), total organic carbon (TOC), total nitrogen (TN), and total organic nitrogen (TON) using a CHNS analyzer (Elementar vario EL cube; detection limit of 1% by mass for each parameter). Additionally, TOC was also measured in additional samples located 13 cm deep from cells #3-6, 3 cm deep from cells #3, #4 and #6, and 17 cm deep from cell #5. This allowed to fully cover the subset of samples selected for the SEDEX procedure (details in A1)

In total, the concentrations of six parameters, *i.e.*, TP, sodium (Na), potassium (K), calcium (Ca), iron (Fe), and manganese (Mn) were measured in all 115 samples. TOC concentrations were measured in 36 samples of which 15 were also used to measure fractional P concentrations with SEDEX. Though TC concentration was measured in 28 samples, only 7 overlapped with the subset used for SEDEX. The way in which each of these different variable combinations were treated is further discussed in Section 2.5

2.3 Total phosphrus (TP)

All soil samples available from the core set were analyzed for TP using the magnesium nitrate ($MgNO_3$) digestion method described by Aspila et al. (1976) since the method corresponds to the final step of the SEDEX and provides comparable results. In this method, concentrated $MgNO_3$ solution (1 g $MgNO_3$ per 1 mL water) was added to 0.1 g soil samples. The samples were then ashed in a muffle furnace at 550°C for 2 hours. After cooling, 10 mL of 1 M hydrochloric acid (HCl) was added, and the soil was resuspended before shaking at 100 rpm for 16 hours. After the extraction was complete, the extracted water samples were filtered through 0.45 µm nylon syringe filters (VWR). One mL of extract was combined with 0.2 µL of concentrated nitric acid (68% Omni Trace HNO_3) for matrix matching and diluted to 10 mL for analysis of major cations including Na, K, Ca, Mn, Fe, and TP using Inductively Coupled Plasma – Optical Emission Spectrometry (ICP-OES, Thermo Scientific iCAP 6300 Duo). Though the inclusion of magnesium nitrate and high temperature ash steps in the TP extraction procedure described above differs from the commonly used EPA acid extraction method (Method 6010C US EPA, 2007, Method 3050B 2019), both methods represent similar TP fractions (Aspila et al., 1976; Spivakov et al., 1999) but may result in minor differences with respect to the values measured. As the aim of this analysis was to discuss the metal concentrations with respect to how TP varied in the bioretention cell system rather than to discuss their standalone concentrations with respect to other published values, the non-standard method used here was adequate.

2.4 Sequential extraction (SEDEX)

The modified SEDEX method (as modified by Baldwin, 1996; originally developed by Ruttenberg, 1992) was used to characterize the distribution of soil TP into different fractions based on release characteristics. SEDEX distinguishes 6 phosphorus fractions (Figure 2): extractable

(P_{Ex}^{I}); humic bound (P_{Hum}^{II}); iron bond (P_{Fe}^{III}); calcium bound (authigenic fluorapatite, biogenic apatite, and carbonate bound (P_{Ca}^{IV}); detrital apatite and inorganic bound (P_{Det}^{V}); and organic/residual (P_{Org}^{VI}) (Baldwin, 1996; O'Connell et al., 2020; Parsons et al., 2017; Ruttenberg et al., 2009). As other sequential extraction methods and even SEDEX can vary in nomenclature (Baldwin, 1996; Ruttenberg, 1992) and chemical characteristics (Spivakov et al., 1999) when referring to specific P fractions hereafter, the step in the SEDEX procedure will be explicitly identified as a superscripted roman numeral.

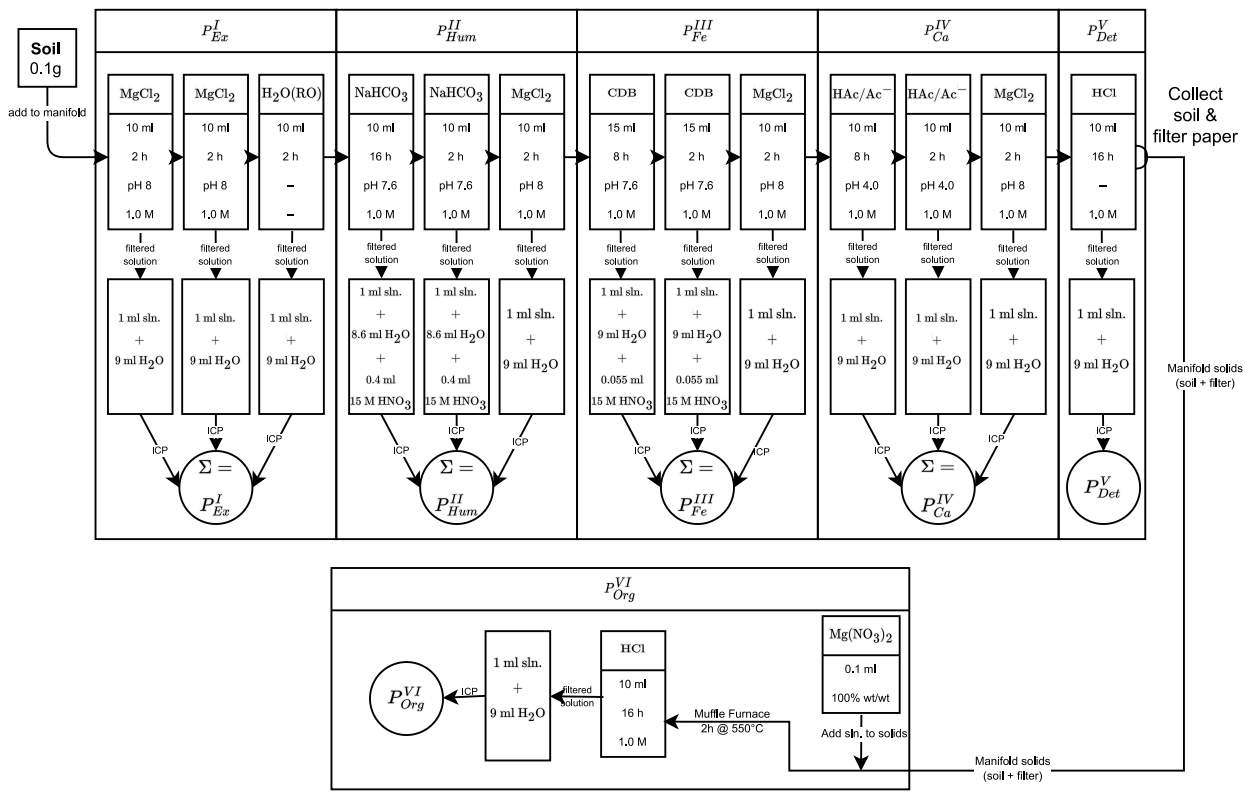

Figure 2: Schematic of the steps used in the modified SEDEX procedure(Baldwin, 1996; Ruttenberg, 1992) for characterizing the distribution of sediment P into different fractions ("Sln" means "solution").

Though the SEDEX procedure distinguishes six different fractions, the extraction steps for the first four fractions require multiple leaching sub-steps with a specific extractant solution and a final

rinse step with either magnesium chloride ($MgCl_2$) or reverse osmosis (RO) water (Milli-Q) (Figure 2). The number of extraction sub-steps in each overall step and their durations were optimized prior to this study to maximize P extraction from the target fraction released during each step. Step 1 of SEDEX used a 1 M $MgCl_2$ extractant to solubilize loosely sorbed, exchangeable P (P_{Ex}^{I}) on the surface of soil minerals by promoting anion exchange with chloride (Cl^-) and formation of Mg-P complexes (Ruttenberg, 1992). RO water was used as the final rinse in this step to remove the remaining solution and P. For all subsequent steps, 1 M $MgCl_2$ solution was used to rinse between extractants instead. Step 2 (suggested by Baldwin, 1996; applied in O'Connell et al., 2020; and Parsons et al., 2017) used a 1 M sodium bicarbonate buffer to leach phosphorus contained in organic, humic acid complexes (P_{Hum}^{II}) to prevent them from co-extracting in the subsequent step. Step 3 used a citrate, dithionate, bicarbonate (CDB) reagent mixture as the extractant. Step 3 targeted P associated with Fe (III) minerals released through reduction with dithionate (P_{Fe}^{III}) while citrate acted as a chelating and buffering agent. Step 4 used an acetic acid/sodium acetate buffer system at pH 4.0 to promote the dissolution of authigenic apatite and other P containing carbonate and calcium minerals (P_{Ca}^{IV}) without dissolving the more recalcitrant inorganic P bound in minerals of detrital origin (P_{Det}^{V}). The final two extractions were both performed with 1 M hydrochloric acid, the first by shaking the mixture and collecting the filtrate as with previous steps and the second, after ashing the soil samples and their filters for 2 hours at 550°C with 100% wt/wt $MgNO_3$ (Aspila et al., 1976). The two extractions targeted the remaining inorganic P (P_{Det}^{V}) and organic/residual phosphorus $\left(P_{Org}^{VI}\right)$ fractions, respectively. For the steps that consisted of more than one extraction, the total sum of P extracted in the individual steps was added to calculate the total P leached during each step (Figure 2). All extract solutions except those collected with Milli-Q water were diluted by a factor of 10 before analysis by ICP-OES and

acidified with 2% HNO_3 to match the carrier fluid of the instrument and reduce matrix effects. A custom manifold (adapted from the design in Ruttenberg et al., 2009) was designed to hold samples and their respective extractants on acid washed 0.45 µm polycarbonate filters throughout the procedure. All other components that came into contact with samples or solutions were made with Polytetrafluoroethylene (PTFE) to reduce interference with extractants and minimize P sorption. All equipment was washed in a P-free citric acid cycle, soaked for 24 hours in a 2-M hydrochloric acid bath, and rinsed with Milli-Q water between uses. All samples used in SEDEX were run in duplicate and concentrations and reported as the mean of both results unless otherwise stated.

2.5 Data and statistical analysis

Since the cores collected from the bioretention cells in 2019 were not deep enough to provide samples of equivalent depths to those reported in the deep (35-45cm) grab sample within pre-existing data, 2019 data were not considered when evaluating changes in TP over time at that depth. For shallow samples (top 10 cm of filter media), TP concentrations of all 2019 samples within the top 10 cm of filter media were averaged to represent the values in the grab samples of the same depth range used for pre-existing data in each of the cells.

The accumulation rate with standard error and 95% confidence intervals were calculated for each individual cell in which pre-existing grab sample data were available, *i.e.,* cells #1, #4, and #6 at the two individual depth ranges (0-10 cm and 35-45 cm) for which s. A simple linear regression ($y = ax+b$) was applied to the filtration media TP concentrations (y) versus time (x, *i.e.,* years since initial sample) and the slope (a) represents the filtration media TP accumulation rate (mgP kg yr^{-1}) as an annual increase in concentration.

For more comprehensive assessments of the multivariate relationships present in the data collected, the data was grouped into various subsets corresponding to the differing number of filtration media samples for which certain analyses were performed. The subsets had 115, 36, 15, and 7 filtration media samples with 6, 7, 13, and 14 different analytical parameters (*e.g.*, concentrations) available, respectively. All subsets except the 115 × 6 set had non-detects (4 × OC < 1% and 5 × P_{Ex}^{I} < 0.6 mgP kg^{-1} values in the dataset), which required the use of censored, non-parametric methods to analyze the censored data (Helsel, 2011) as ordinal values. Though no variables with non-detects were included in the 6 element concentrations measured in all 115 filtration media samples, non-parametric methods were still used for multivariate analysis as there was a likelihood that data may not have fit the necessary distribution characteristics (Helsel et al., 2020). Least squares linear regressions and Pearson correlation coefficients (a parametric method) were only used to better quantify relationships between pairs of variables where data was normally distributed, free of non-detects and showed evidence of linear correlation without requiring transformation. A "line of organic correlation" (Helsel et al., 2020), between molal Fe and Mn was used instead of an ordinary least squares regression to estimate the Fe:Mn ratio that both elemental concentrations varied within our samples in an equally biased manner.

The two primary methods used to identify the multivariate relationships were pairwise Spearman correlations between the variables and nonmetric multidimensional scaling (NMDS) using Euclidean distance between the ranks (Helsel, 2011, p. 284) using the *R* package: `vegan` (Oksanen et al., 2020). In addition to ranked concentration values for each sample, variables for both cell position and depth were included in the NMDS data. The predictor variables were then plotted with respect to the two primary NMDS component weights to identify clustering of correlated variables. NMDS was not performed on the 7×14 subset of results as 7 samples were

insufficient to assess relationships between 16 variables (14 concentration variables, cell # variable, and a depth variable).

As is commonly done with principal component analysis (PCA), variables were plotted with respect to the two primary components. Clustering of variables when plotted this way identifies covariation. Unlike PCA, the non-parametric nature of the test and conversion to rank values in the data mean that the absolute magnitudes of component values are not meaningful (Helsel, 2011). The conversion to ordinal (ranked) values in the process (required to properly handle non-detects) means that it provides primarily directional variation tendencies within the data, *i.e.* "higher values of X are more likely to be found in samples with higher values of Y where ordinal position within the dataset and not magnitude/ratio constitutes a 'higher' value".

3 Results

3.1 Total Phosphorus

The filtration media TP concentrations increased over time in the bioretention cells (Figure 3). From the pre-existing data (Credit Valley Conservation, 2016) for cells #1, #4, and #6, the mean TP concentrations in the top 5 cm of the cells were 333 ± 76 mgP kg^{-1} in 2013 (n = 3), 320 ± 20 mgP kg^{-1} in 2014 (n = 3), 467 ± 25 mgP kg^{-1} in 2016 (n = 3), and 733 ± 142 mgP kg^{-1} in 2019 (n = 35) (Figure 4). The filtration media TP accumulation rates were approximately 2 times greater near the surface than in the deeper filtration media horizon, ranging from 67 to 78 mgP kg^{-1} yr^{-1} in the top 10 cm and from 4.2 to 40 mgP kg^{-1} yr^{-1} in 35-45 cm below the filtration media surface (Figure 3).

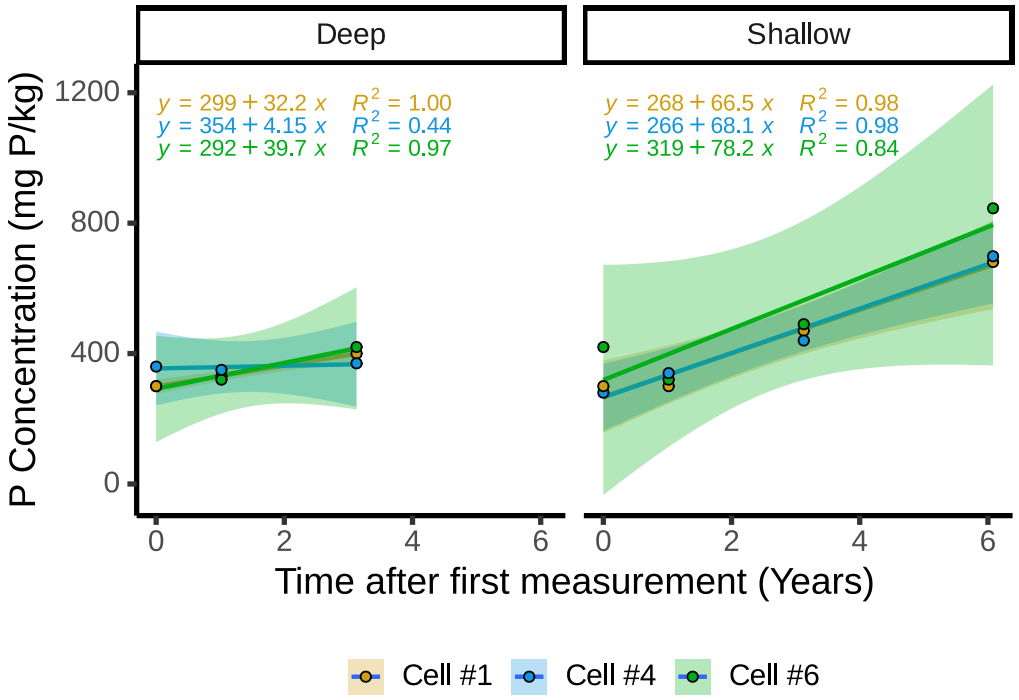

Figure 3: Linear models (ax + b) with equations and 95% confidence intervals are shown for individual cells. Slope (a) represents yearly accumulation rates per kilogram of filtration media (mgP kg $media^{-1}year^{-1}$). Samples from 2016 (year 3) and prior are grab samples reported in a CVC

technical report (Credit Valley Conservation, 2016). Corresponding values in 2019 core samples are averages of TP concentrations nearest to the associated region (0-10 cm for shallow; NA for deep).

When comparing TP concentrations in the depths available for all 12 cores collected in 2019 (*i.e.*, 0-10 cm), cells #1 to #5 all had similar concentrations (in the range of 607 to 674 mgP kg^{-1}) and variability (standard deviation (sd) = 82-170 mgP kg^{-1}) while cell #6 showed significantly higher TP concentrations and variability (745 ± 238 mgP kg^{-1}) (Figure 4). The vertical distribution pattern of TP concentrations in cell #6 was also different from that in the other bioretention cells. In bioretention cells #1 to #5, TP concentrations were constant over the top 17 cm of the filtration media profiles and exhibited a decrease deeper down. In bioretention cell #6, and especially core #2 within it, TP concentrations peaked to ~1,100 mgP kg^{-1} at depths 6-10 cm below the filtration media surface, while they were lower at the surface (650-850 mgP kg^{-1}; see Figure 4). Note that due to the shallow depth investigated, less than 25 cm deep, only the deeper cores exhibited significant vertical decreases with depth.

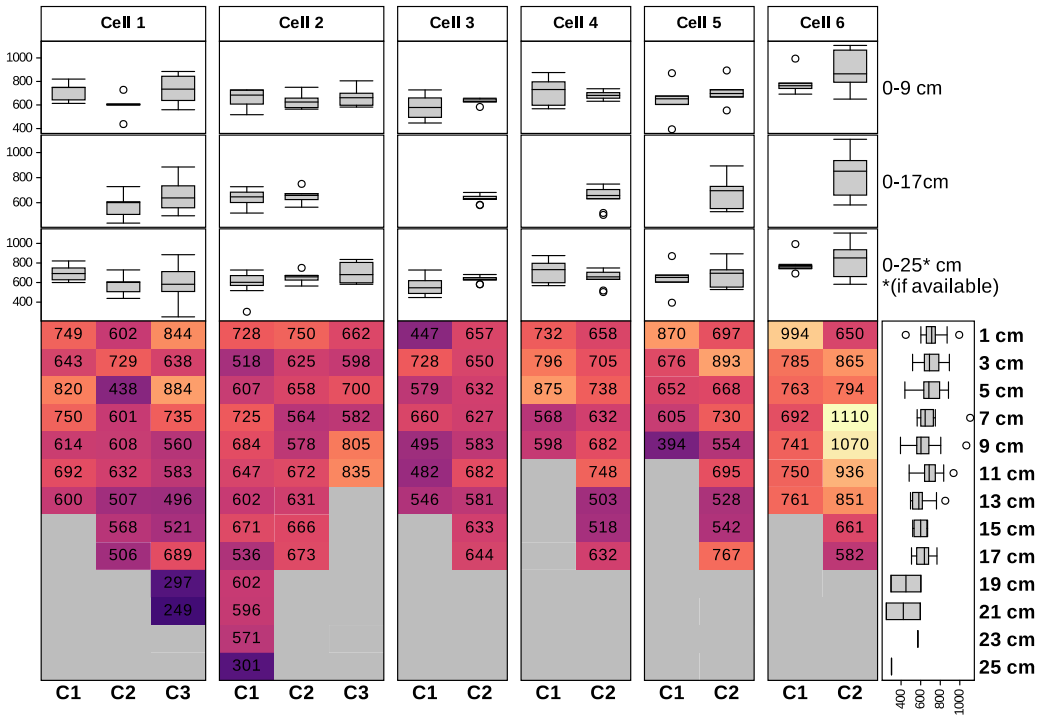

Figure 4: Phosphorus concentrations in slices of core samples taken from the bioretention cells in 2019 (i.e., 7 years post-construction). Boxplots summarize distributions of concentrations by depth (right) and core (top) for samples in the corresponding row/column. Per-core boxplots (above table) shown for top 10 cm of all cores (top row), top 17 cm of cores more than 17 cm deep (middle row) and all samples within the cores (bottom row). Depths shown represent center points of 2cm slices (*i.e.* a 3 cm depth represents a slice covering the 2-4 cm depth range) below the surface of filtration media.

3.2 Carbon and nitrogen

TN and TON concentrations in all samples were below 1% N by weight, the detection limit of the instrument. Stratification was observed in the TC depth profile of the cores and was primarily driven by decreasing TOC concentrations as depth increased (Figure 5). The inorganic fraction of the samples (4.8 ± 1.2 %) did not vary significantly between cores or with depth. TOC was highest (11.5%) at the surface and rapidly decreased in the top 7 cm of the filtration media to just over 1%; *i.e.*, the method detection limit. Five samples in the overall dataset including one in the deepest core (shown in Figure 5) had TOC below the detection limit. Compared to the overall decreasing

trend and spatially adjacent measurements, an abnormally high amount of TOC (4.9%) was measured at a depth of 17 cm in core #1 of cell #2 (shown in Figure 5), which was confirmed by analyzing a duplicate sample (6.3%). The only other sample available from cell #2 at an equivalent depth (core #2) had no detectable TOC. At the surface, TOC accounted for 66-71% (*n* = 3) of TC and rapidly decreased in the top 11 cm to less than 2% OC.

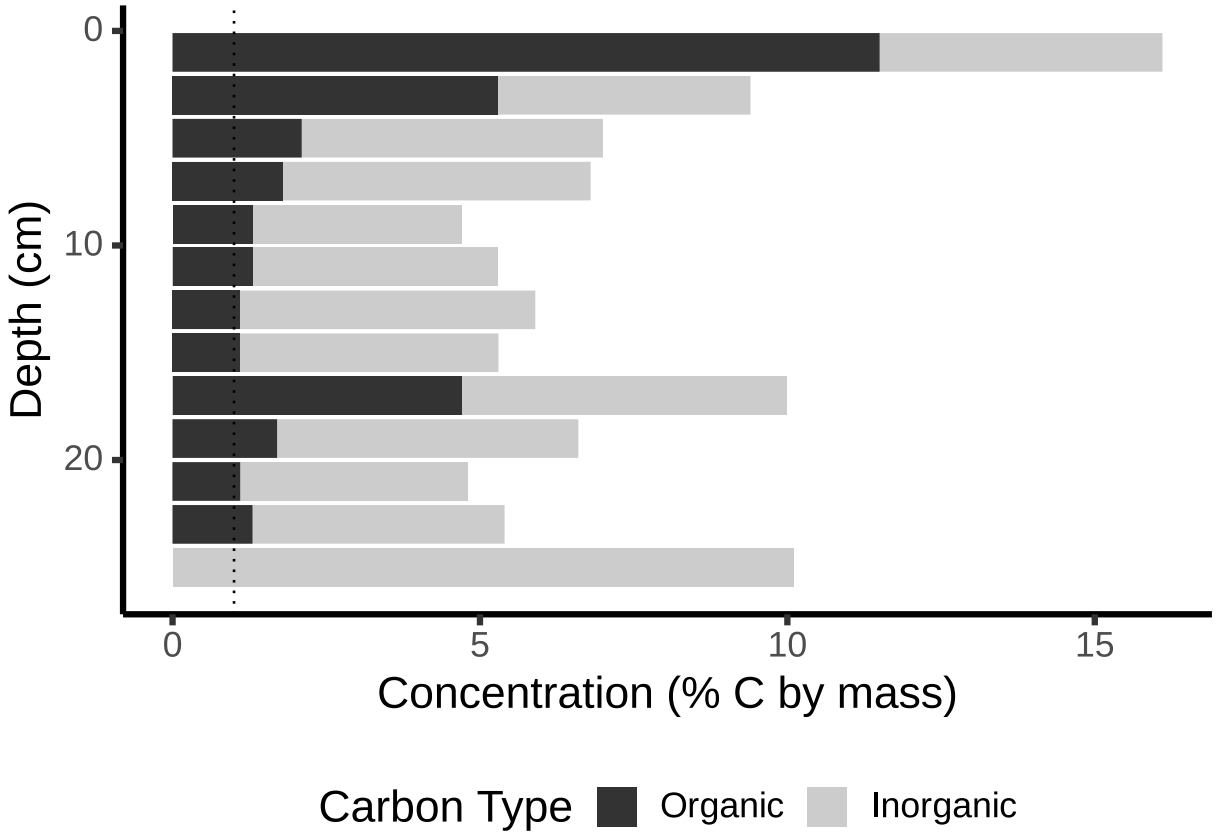

Figure 5: Concentrations of organic and inorganic carbon in filtration media samples from cell #2, core #1. Method detection limits (1% for both TC and TOC) are shown with a dashed line (n = 1 for all samples).

3.3 Phosphorus Fractions

The concentrations present in the 6 P fractions measured using SEDEX and the proportion of TP they represented varied throughout the samples measured in the system (Table S5-1). In samples

from the top 5 cm, concentrations of P_{Ex}^{I}, P_{Hum}^{II}, and P_{Org}^{VI} all represented greater proportions of TP (1-5%, 4-15%, and 10-22%, respectively) than in samples from deeper zones (<0.1%, 3-10%, and 8-18%, respectively, in samples at depth 13-17 cm). Concentrations in P_{Fe}^{III} showed more complex relationship with depth (discussed further in sections 3.4 and 4.3.2) contributing between 9% and 31% of the TP in the samples measured. Absolute concentrations in P_{Ca}^{IV} and P_{Det}^{V}remained relatively consistent throughout the samples at 67-119 and 118-382 mgP kg^{-1}, respectively. However, deeper samples had decreased concentrations in the other fractions (P_{Ex}^{I}, P_{Hum}^{II}, P_{Fe}^{III}, and P_{Org}^{VI}) therefore proportional composition of TP was more biased towards Ca associated fractions (P_{Ca}^{IV} and P_{Det}^{V}). Proportionally, TP was 10-19% P_{Ca}^{IV} and 28-55% P_{Det}^{V}, above 5cm; and 11-23% P_{Ca}^{IV} and 33-56% for P_{Det}^{V} below 13 cm. The relationships observed between variation in fractional concentrations and other environmental parameters measured in the samples will be discussed in more detail below.

Soil samples closer to the surface of cell #2 were proportionally higher in more labile and organic-related P fractions (*i.e.*, exchangeable P (P_{Ex}^{I}), humic bound P (P_{Hum}^{II}), and residual/organic P (P_{Org}^{VI}) fractions) than those deeper in the core (Figure 6 and Table A6-1). In contrast, mineral-bound P fractions, particularly the calcium-related, tightly-bound, P fractions associated with detrital calcium minerals (P_{Det}^{V}) and authigenic apatite adsorption/precipitation (P_{Ca}^{IV}) minerals did not exhibit a clear relationship with sample depth. However, absolute concentrations of P in these fractions remained relatively stable and the proportional shift was primarily driven by a decrease in the other fractions (P_{Ex}^{I}, P_{Hum}^{II}, P_{Fe}^{III}, and P_{Org}^{VI}) as depth increased. Notably, a reduction in the concentrations of redox-sensitive Fe-associated P (P_{Fe}^{III}) was observed in the deepest sample (25

cm) analyzed but otherwise remained relatively constant in proportion throughout the rest of the filtration media profile.

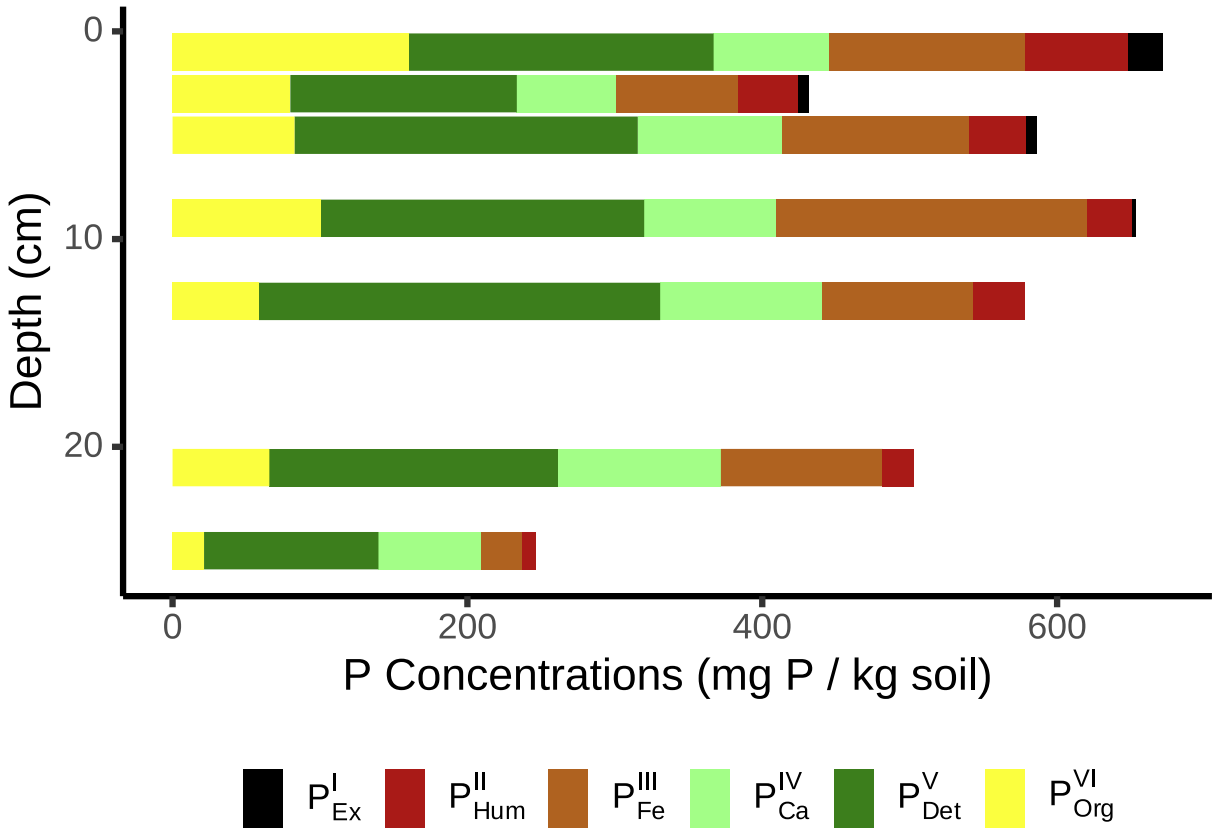

Figure 6: Total concentrations of different phosphorus fractions in bioretention cell #2, core #1 collected in November 2019.

On average, the difference between TP estimated as the sum of all SEDEX fractional concentrations was 26±44 mgP L^{-1} (5±8%) lower than the directly measured TP (Aspila et al., 1976) in the samples.

3.4 Parameter clustering in non-metric dimensional scaling (NMDS)

Multivariate analysis using NMDS and Euclidean distance between rankings for each variable produced convergent solutions for three of the four possible sets of variables. All three solutions

converged to stable results with well characterized distributions of error. Biplots of the two primary components in each of the three subsets for which NMDS produced solutions are shown in Figure 7 to illustrate clustering and co-variation in the data.

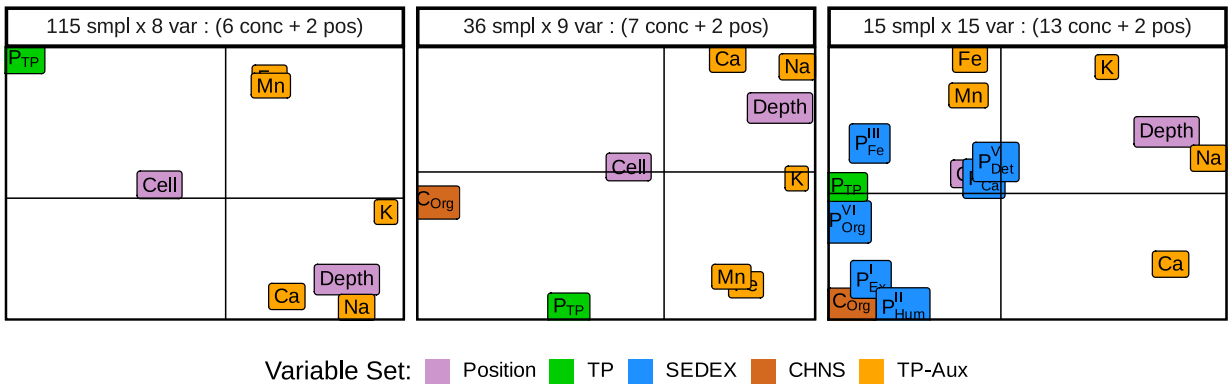

Figure 7: NMDS biplots of 6, 7, and 13 parameters measured in the samples (n=115, 36 and 15, respectively). Colours are used to parameters analyzed/measured together. 'Pos' variables (i.e., positions as Depth and Cell #) were included in the analysis.

In all three set of variables, TP concentration was well represented in at least one (15 samples ×15 variables) or both (115 samples × 8 variables and 36 samples × 9 variables) of the principal components. Three clusters of variables associated with TP concentration were evident in the data. TP had a positive relationship with 1) redox-associated compounds including Fe and Mn concentrations and 2) OC concentrations, and a negative relationship with Ca, K, Na, and depth. In all three cases, Fe and Mn concentrations clustered together indicating tight covariation. The Fe+Mn cluster and TP concentrations were in the same principal component in all three data groupings (6, 7, and 14 available parameters). In the 15 samples where fractional SEDEX concentrations were measured, TP and P_{Fe}^{III} concentrations clustered most closely with Fe, and Mn concentrations (see Figure 7). In the biplots of samples for which there were both fractional SEDEX and carbon concentration data, C_{org} concentrations were found to cluster near TP

concentrations on the other side of Fe and Mn concentrations. In the 15 samples with SEDEX fractions, P_{Ex}^{I} , P_{Hum}^{II}, and P_{Org}^{VI} concentrations clustered closest to C_{org} concentrations. Opposite to this cluster, indicating inverse trends in variation, a cluster of K, Ca, and Na concentrations and sample depth was present (in both the 15 variable- and 9 variable-sets). Neither P_{Ca}^{IV} or P_{Det}^{V} concentrations clustered with TP concentrations, Ca concentrations or any of the other parameters analyzed in the system.

To identify which of these (pairwise) relationships were significant, selected regressions between variable pairs are presented below. In the set containing all 115 samples (presented in full in Section S4), the filtration media depth and concentrations of K, Na, and Ca in filtration media were found to vary inversely to TP concentrations. Fe and Mn concentrations co-varied linearly (Figure A5-1) with each other (Pearson's R^2=0.88, p<0.001) and with TP concentrations to a lesser degree (Pearson's R^2=0.48 for Fe and 0.42 for Mn, p<0.001). The line of organic correlation for molal (mmol kg^{-1}) concentrations of Fe with respect to Mn was found to be: $[Fe] = 22.6 \frac{mol\ Mn}{mol\ Fe} \times [Mn] - 75.6\ mmol$ Fe Kg^{-1} with a mean molar Fe:Mn ratio of 15±2 in the samples. TP concentrations were found to also vary with C_{org} concentrations (Spearman ρ = 0.40 p<0.1 used due to non-detects) in the 36 samples where both concentrations were measured. However, there was no significant relationship (p>0.1) between C_{org} concentrations and Fe or Mn concentrations.

4 Discussion

4.1 Field estimates of P accumulation rates

The first major result of this study is the estimation of field-based P accumulation rates in the six-cell bioretention system using up to four timepoints. These data showed that on average, the yearly rates of P accumulation in the filtration media were 70.9 ± 8.6 mgP kg^{-1} y^{-1} (top) and 25.4 ± 6.4 mgP kg^{-1} y^{-1} (within the media, at 25-30 cm deep). The corresponding areal P accumulation rate at 25-30 cm depth, assuming a bulk density of 1,600 kg m^{-3}, was 18.3 ± 4.6 gP m^{-2} y^{-1} or 183 ± 46 kgP ha^{-1} y^{-1}. Very few data exist in the literature on the field accumulation of P in bioretention filtration media from TP filtration media measurements over time (for examples see: Goor et al., 2021; Komlos and Traver, 2012). The relationships we obtained (Figure 3) suggest that TP accumulation in filtration media is linear over time, at least over the first 7 years following construction. Therefore, we assumed such a linear relationship for other systems and used other published filtration media TP concentrations for bioretention systems for which TP were obtained at two time points to estimate TP accumulation rates. For example, Johnson and Hunt (2016) measured Mehlich-3 P (M3-P) concentration in a bioretention cell located in Charlotte, NC following construction and 11 years later. Once converted to TP concentrations using the Lammers and Bledsoe's equation (*i.e.,* M3-P = 0.117 × TP) (Lammers and Bledsoe, 2017), and assuming a linear increase in filtration media TP between these two time points, the bioretention cell of their study accumulated 14.9 mgP kg^{-1} y^{-1}, which agrees very well with our estimates. Using data of the same authors from another study of a bioretention cell in Chapel Hill, NC (Johnson and Hunt, 2019), we calculated an accumulation rate at 9 mgP kg^{-1} y^{-1} over 17 years. Most studies do not provide filtration media TP concentration over time, and rather focus on measuring dissolved P concentrations in the inflow and outflow of a bioretention cell to calculate percent removal (*i.e.,*

concentration or mass decreases through the system). Using various assumptions, *e.g.*, on runoff volume, P concentrations, and bulk density, Davis et al. 2006 estimated a filtration media P accumulation rate at 5.3 mgP kg^{-1} y^{-1}, which is within an order of magnitude of our field estimates. The bioretention cells in our study, like the ones utilized by Johnson and Hunt (2016, 2019), were conventionally designed, *i.e.*, made of unamended sandy media, vegetated, and without an internal water storage zone. As such, these cells are representative of many existing systems. Until better filtration media TP concentration *vs.* time relationships (other than a linear one) and estimates are obtained, we suggest the use of P accumulation rates at 10 to 40 mgP kg^{-1} y^{-1} within the filtration media of such conventionally-designed bioretention cells and approximately twice as much on the top 5 cm. There is a need for more time-dependent filtration media TP data in bioretention cells, to get a tighter range of such estimates under realistic field conditions and for different bioretention cell designs. Such data should be obtained over longer periods of time to estimate the length of the linear range of P accumulation and identify when P saturation can be expected.

These field-estimated P accumulation rates are critical to predict the lifetime of bioretention cells for P retention. However, estimation of when, how, and where P accumulation occurs within bioretention systems has suffered from a few key limitations so far and has often been omitted from models due to complexity (Li et al., 2018) and lack of easily comparable data (Johnson and Hunt, 2019; Manka et al., 2016). The main inclusion of P accumulation within bioretention systems has been in models derived from lab-scale column and mesocosms studies (Li and Davis, 2016a; Li et al., 2021; Luo et al., 2020; Marvin et al., 2020; Spraakman, 2021), which almost universally substitute direct measurement of changes in P content within filtration media with estimation from inflow/outflow concentration-volume derived loadings. Though rates of P adsorption, and, sometimes, vegetation uptake of P and leaching from particulate P and/or organic

matter to dissolved P are conceptually discussed alongside existing models (Aladesote and Hunter, 2020; Li et al., 2018; Li and Davis, 2016a, 2016b; Manka et al., 2016), the processes are at most included as fixed empirical coefficients or entirely omitted in the implementations presented. However, some notable exceptions to the norms above exist. For example, some models include adsorption rates calculated based on an assumed first-order adsorption rate constant determined from laboratory experiments (Brown and Hunt, 2011; Goor et al., 2021; Li and Davis, 2016b; Liu et al., 2021) or vegetation uptake rates empirically derived from a mass balance (Glaister et al., 2014; Muerdter et al., 2016). The herein presented field estimates of P accumulation rates could be substituted for calculated adsorption, leaching and plant uptake rates.

4.2 Evidence of unsaturated cell media

The linear increase in filtration media TP concentrations over time throughout the media presents clear evidence of continued P accumulation in the bioretention cells even 7 years post-construction (2012-2019), as previously also reported (Guo et al., 2019; Hsieh et al., 2007; Johnson and Hunt, 2019; Kandel, 2016; Kandel et al., 2017; Komlos and Traver, 2012; Liu et al., 2021; Marvin et al., 2020). The "low phosphorus index" initially specified for the media during construction (Credit Valley Conservation, 2016, verified by personal communication) – though never quantified – suggests an initially low level of TP in the filtration media. The initial TP concentrations measured in 2014 in our system, at 327 +/- 17 mgP kg^{-1}, were significantly higher than those reported for sandy bioretention media immediately post-construction in other systems, *e.g.*, at 32-144 mgP kg^{-1} (Johnson and Hunt, 2016) that followed design guidelines for building bioretention cells with filtration media that exhibit a low P-index, between 10 and 30 ppm (Hunt et al., 2006a). Despite the higher initial concentrations, correspondingly higher input TP loading (*e.g.* > 3 mg P L^{-1}

reported in Goor et al., 2021) at our field site may have resulted in the strong capacity of the system to accumulate runoff-laden P that we observed.

The vertical distribution of P in the bioretention cell filtration media, especially in cells #1 to #5, was consistent with previous studies that also reported the largest TP concentrations and annual accumulation rates closer to the filtration media surface (Figure 4 and Figure 3) (Brown and Hunt, 2011; Johnson and Hunt, 2019; Li and Davis, 2016b). These patterns suggest the adsorption of dissolved P to organic material and sedimentation of P-laden particles in the top portion of the filtration media, and some migration of P-laden particles from the top down to deeper horizons. Along with the above-mentioned increase in P accumulation over time, both in the top of the bioretention media, and, to a lower extent, in deeper zones, these results showed that the bioretention cell continued to accumulate P within its media.

Filtration media P accumulation at the surface is expected until TP filtration media concentrations are at equilibrium with inflow TP concentrations. The filtration models proposed by Davis *et al.* (2016) for total suspended solids (TSS) and their associated TP load suggested an approximately exponential decrease in concentration with increasing depth prior to reaching equilibrium at the surface. While the overall trends we observed follow predictions from this model, the exponential nature of filtration media TP concentration was not evident in our data. This can be explained by the fact that our data were obtained from a shallow profile in the field and not in controlled soil column experiments. This top filtration media zone was also subject to freeze-thaw cycles, which are common in this region in the winter. In our previous study, freeze-thaw cycles were shown to slightly reduce P adsorption (Ding et al., 2019) which likely partly explain that P filtration media saturation was not yet reached after 7 years. In the field, uncontrolled physical, biogeochemical, and climatic factors result in more variability in filtration media TP

concentrations than in controlled laboratory filtration media column experiments. In addition, field studies do not allow the high depth- and time-dependent data frequency that would be required to exhibit a specific mathematical model (*i.e.*, exponential trends). A number of contributing factors that are consistent with our more detailed fractional P results will be discussed in the following section.

Cell #6, the most downstream cell, had significantly higher TP concentrations in our samples (Figure 4), a TP peak lower than in the other cells, and the highest TP accumulation rate (Figure 3). The first explanation for these observations is that cell #6 was located on the corner of two streets (rather than just one as for the other cells) and it received a larger volume of stormwater runoff due to a larger associated watershed. These factors likely contributed more input P compared to the other cells. The second explanation is related to its uncommon plumbing: cells #3 to 6 were hydraulically connected through a common underdrain, with the effluent of cell #3 being mixed with that of cell #4, subsequently with that of cell #5, and cell #6 receiving the effluent of all 3 previous cells in its underdrain (Figure 1b). The subsurface peak in TP observed in cell #6 might be due to upstream cell effluent backwashing within cell #6 during high-intensity events. This likely resulted in upstream P redepositing within the media of cell #6, thus explaining the TP peak observed at 7 to 9 cm deep.

4.3 Potential organic and inorganic drivers of TP distribution

The second major result of this work is the identification and quantification of P fractions across the vertical profiles of the bioretention cell media layers. Phosphorus can sorb on and desorb from Fe- and Al-oxides and clay and Ca minerals; P can precipitate as or be released to the water from various minerals such as Ca-based hydroxyapatite [$Ca_5(PO_4)_3OH$] and tricalcium phosphate [$Ca_3(PO_4)_2$] and Fe-based strengite [$FePO_4.2H_2O$] and vivianite [$Fe_3(PO_4)_2.8H_2O$]; and P can be

produced from the mineralization of P-containing organic matter and be taken up by and incorporated in plant and microbial cells (Li et al., 2021; Liu and Davis, 2014; Marvin et al., 2020; Roy-Poirier et al., 2010; Zhang et al., 2021). These processes depend on redox and pH conditions as well as plant and microbial activity, all of which may vary seasonally. Overall, the differences in accumulation patterns observed for the various P fractions analyzed represent the combined differences in upstream sources and P retention and transformation mechanisms.

4.3.1 TP associated with near-surface organic matter

Though the filtration media analyses performed in this study are insufficient to identify the specific processes responsible for TP behavior in our study site, they provide evidence for links between TP and organic material within the filtration media. We observed a positive correlation between filtration media TP and organic carbon (OC) as well as correlations of OC with P_{Ex}^{I}, P_{Hum}^{II} and P_{Org}^{VI} (Figure 7 and below). These correlations were particularly apparent in the near-surface environment.

P_{Ex}^{I} represented the smallest proportion of these three fractions and was only detectable (*i.e.* > 0.61 mg kg^{-1}) in the top 5 cm. Though its not nominally associated with organic matter, P_{Ex}^{I} also includes a portion of P associated with biogenic $CaCO_3$ and has been previously reported to include some P within plankton (Parsons et al., 2017; Ruttenberg, 1992), which suggests some P contained in microorganisms may also be included. Therefore, the presence of P_{Ex}^{I} in the surface may be evidence of two main sources: First, P in recently filtered 'fresh' particulates containing loosely bound P that has not yet been weathered. Second, a portion of P associated with microbial activity in the oxygen and organic-matter-rich near-surface region of the filtration media.

The presence and even distribution of P in P_{Hum}^{II} and P_{Org}^{VI} suggests that both fractions had relevant impacts on the overall P retention characteristics of the cells. Though organic molecules play a role in both of these fractions, P_{Hum}^{II} primarily reflects phosphate present in complexes involving humic acids and a bridging cation (Fe^{3+}, Al^{3+}, Zn^{2+} Ca^{2+}, *etc.*) while P_{Org}^{VI} reflects P included within organic molecules themselves (Guardado et al., 2007; Parsons et al., 2017; Ruttenberg, 1992). As both fractions are present in approximately equal quantities, this suggests that both the weathered residues associated with P_{Hum}^{II} and the 'fresher' organic molecules associated with P_{Org}^{VI} affect the P retention within bioretention cells with neither one being the obviously dominant form of retention. The strong correlation between all three fractions (P_{Ex}^{I}, P_{Hum}^{II}, and P_{Org}^{VI}) and OC (Figure 7 and Figure A5-2) further supports the hypothesis that in the near-surface environment of the cell, the P retention characteristics we observed in the system are strongly related to organic activity within the system.

4.3.2 Role of Fe and Mn in deeper regions

Fe based additives have comprised a large portion of the strategies employed to enhance P retention characteristics of bioretention cells (Marvin et al., 2020; Yang and Lusk, 2018; Zhang et al., 2018). Our data showed strong positive correlation between TP, Mn, and Fe concentrations. This correlation was further corroborated by the correlation of all three concentrations with P_{Fe}^{III} further supporting the hypothesis that Fe and Mn related processes are involved in the P biogeochemistry of the bioretention media.

The strong correlation between Fe and Mn concentrations in our system limits the possibility of separately identifying their impacts. However, the good linear fit between both variables provides some insights into potential causes of co-variation in the system. The line of organic correlation

between Fe and Mn indicates that they co-varied at a molar ratio of 22.6:1 (*i.e.* a change in one mole of Mn corresponded to a change in 22.6 additional mole Fe). This value is different from the overall Fe:Mn molar ratio observed (Fe:Mn ~15) suggesting that more than one mineral/equilibrium resulted in the distribution observed. As the relationships derived from NMDS only rely on the similarities in changes between parameters, the process linking changes in TP and P_{Fe}^{III} with those in Fe and Mn in the samples would have been more likely to reflect the former (ΔFe:ΔMn = 22.6) of the two ratios presented. While Fe:Al concentrations and ratios have previously been reported to have an impact on P capture within bioretention media (Zhang et al., 2018), similar ratios have not yet been reported for Fe:Mn.

Studies of prolonged flooding in agricultural soils have previously found that reducing, anaerobic conditions during prolonged flooding can result in solubilization of P associated with Fe and Mn (Concepcion et al., 2021; Gregory et al., 2017), an effect also seldom observed in bioretention cells (Shetterly, 2018). A column experiment (Glaister et al., 2014) found that inclusion of a saturated, organic-rich zone in their systems did not significantly affect overall TP removal and speculated that Fe reduction leading to release of bound P did not occur.

4.3.3 Impact of Ca, Na and K

We observed relatively high concentrations in Na and Ca, ranging from 200 to 2,000 mgNa kg^{-1} (Figure A2-10) and 82-183 gCa kg^{-1} (Figure A2-12), which may be explained by location of the study site in an area subject to significant de-icing salt use during the winter (Burgis et al., 2020; Radosavljevic et al., 2022; Sansalone and Buchberger, 1996). Similar filtration media Na concentrations were observed in bioretention media from similar cold regions (Burgis et al., 2020; Denich et al., 2013; McManus and Davis, 2020), whereas lower concentrations were found in the media of bioretention cells located in more temperate regions with warmer winter (and therefore

no or limited salt applications). The cell media therefore showed evidence of accumulation in Ca, Mg, K, and Na over time (Figure A3-1).

The inverse correlation that we found between TP and K, Na, and Ca suggests that increasing the cation exchange capacity (CEC) decreases the TP content. This is counter-intuitive, as design guidelines recommended a CEC larger than 10 meq/100g (*i.e.*, 10 cmol(+)/kg) at construction (CVC and TRCA, 2010). This result can be explained by the media's initially low CEC (< 10 cmol(+)/kg in 2016) pointing to few cations available for P binding (Hunt et al., 2006).

This finding conflicts with those from a previous bioretention filtration media column experiment in which simulated runoff (with added salt) was injected (Denich et al., 2013). However, these differences might be explained by the significantly higher initial media P content, at 2.235 g P kg^{-1}, in Denich et al.'s compared to the low P-index reported for our bioretention cells: the measured filtration media TP in our study was an order of magnitude lower than in Denich et al.'s (327 +/- 17 mgP kg^{-1} in our system in 2014).

Another counterintuitive result observed within our samples was that variations in Ca concentrations showed no significant relationship with the P fractions most closely related to Ca mechanisms in filtration media (P_{Ca}^{IV} and P_{Det}^{V}). It suggests that the factors driving soil Ca concentration distributions are different and independent from those explaining its associated P fractions (P_{Ca}^{IV} and P_{Det}^{V}). P_{Ca}^{IV} and P_{Det}^{V} did not co-vary with most other spatial and chemical parameters in the core samples where they were measured (Figure 7 and Figure A5-2). This suggests that their concentrations are a result of initial P content within the media.

5 Conclusions

Our study provided direct evidence and quantities of TP accumulation in bioretention cells. All six fractions were present in significant quantities and showed spatially heterogenous distribution patterns providing evidence for complex P behavior within the system. Our findings also suggest that the distributions are likely to also change over time in addition to the horizontal and vertical variability we observed. How fractional P composition varies in bioretention systems as a result of changing environmental conditions and increasing age remains largely unknown and should be further explored in future research

5.1 Implications and Recommendations

The net import observed in the filtration media of our system throughout our study period is evidence that it continued to be capable of TP capture despite its age (7 years). Though some other systems of this age had been suspected to near saturation (Johnson and Hunt, 2020), there were no clear indicators (*i.e.*, tendency towards lower TP accumulation rate) that our system was approaching saturation as of the last samples collected at our site. This is especially encouraging since our site did not employ any specialized media amendments targeted at increasing the filtration media's overall capacity to retain P.

Though elevated P concentrations closer to the surface of the cell were supported by the statistical analyses we performed, the pattern was not as apparent in TP concentrations as it was in concentrations of those P fractions most associated with OC (P_{Ex}^{I}, P_{Hum}^{II} and P_{Org}^{VI}). Therefore, surface media removal and plant harvesting would be most effective at removing accumulated TP with these fractions.

Though a short term column study representative of ‘young’ cells suggested that TP retention was not affected by submersion(Glaister et al., 2014), our evidence for continued accumulation of TP in reduction-sensitive fractions suggests that risk of release under submerged conditions should continue to be evaluated as systems age. This is of particularly important in regions where extreme flooding events are predicted to increase in frequency as a result of climate change. Future studies should investigate fractional P changes in bioretention media during prolonged submersion periods to evaluate potential release of Fe-associated P.

Our study showed evidence suggesting that adsorption onto and, formation or dissolution of Ca minerals did not likely play a major role in the distribution of P in the bioretention media. This suggests that amendments targeting these mechanisms have less potential to be effective than those attempting to improve TP retention in Fe or OC based fractions. Further, Ca, Na, and K concentrations were all found to negatively correlate with overall TP retention potentially suggesting that they may have inhibited processes that promoted it. As both Na and Ca are cations associated with winter de-icing salts commonly used in the region, future research should provide definitive evidence for the effect of salinity on P retention in bioretention cells.

Finally, our data show evidence that comparison across two different methods (that represent different fractional compositions) using a constant/fixed ratio to do so (as suggested in Lammers and Bledsoe, 2017) will introduce undesired influence as a result of varying fractional soil content between samples. As comparisons of results determined using differing methods are likely inevitable due to the fragmented nature of testing methodologies (Dayton et al., 2017; Kleinman et al., 2007; Spraakman et al., 2020), the assumptions inherent in each testing method and their associated caveats should clear before comparing TP concentrations measured or calculated from different methods.

References

Aspila, K.I., Agemian, H., Chau, A.S.Y.Y., 1976. A semi-automated method for the determination of inorganic, organic and total phosphate in sediments. The Analyst 101, 187. https://doi.org/10.1039/an9760100187

Baldwin, D.S., 1996. The phosphorus composition of a diverse series of Australian sediments, Hydrobiologia.

Blecken, G.-T., Zinger, Y., Deletić, A., Fletcher, T.D., Hedström, A., Viklander, M., 2010. Laboratory study on stormwater biofiltration: Nutrient and sediment removal in cold temperatures. J. Hydrol. 394, 507–514. https://doi.org/10.1016/j.jhydrol.2010.10.010

Brezonik, P.L., Stadelmann, T.H., 2002. Analysis and predictive models of stormwater runoff volumes, loads, and pollutant concentrations from watersheds in the Twin Cities metropolitan area, Minnesota, USA. Water Res. 36, 1743–1757. https://doi.org/10.1016/S0043-1354(01)00375-X

Brown, R.A., Hunt, W.F., 2011. Impacts of Media Depth on Effluent Water Quality and Hydrologic Performance of Undersized Bioretention Cells. J. Irrig. Drain. Eng. 137, 132–143. https://doi.org/10.1061/(ASCE)IR.1943-4774.0000167

Burgis, C.R., Hayes, G.M., Henderson, D.A., Zhang, W., Smith, J.A., 2020. Green stormwater infrastructure redirects deicing salt from surface water to groundwater. Sci. Total Environ. 729, 138736. https://doi.org/10.1016/j.scitotenv.2020.138736

Canadian Council of Ministers of the Environment, 2004. Canadian water quality guidelines for the protection of aquatic life: Phosphorus: Canadian Guidance Framework for the Management of Freshwater Systems, in: Canadian Environmental Quality Guidelines. Canadian Council of Ministers of the Environment, Winnipeg.

Concepcion, A., Kumaragamage, D., Akinremi, W., Dharmakeerthi, S., Goltz, D., Indraratne, S., 2021. Phosphorus release from intact soil monoliths of manure-amended fields under simulated snowmelt flooding. J. Environ. Qual. 50, 252–263. https://doi.org/10.1002/jeq2.20179

Credit Valley Conservation, 2016. CVC LID Demonstration Monitoring Projects:Elm Drive Technical Site Report 2011-2015. Missisauga.

CVC, TRCA, 2010. Low impact development stormwater management planning and design guide.

Davis, A.P., 2008. Field Performance of Bioretention: Hydrology Impacts. J. Hydrol. Eng. 13, 90–95. https://doi.org/10.1061/(ASCE)1084-0699(2008)13:2(90)

Davis, A.P., Hunt, W.F., Traver, R.G., Clar, M., 2009. Bioretention technology: Overview of current practice and future needs. J. Environ. Eng. 135, 109–117. https://doi.org/10.1061/(ASCE)0733-9372(2009)135:3(109)

Dayton, E.A., Whitacre, S., Holloman, C., 2017. Comparison of three persulfate digestion methods for total phosphorus analysis and estimation of suspended sediments. Appl. Geochem. 78, 357–362. https://doi.org/10.1016/j.apgeochem.2017.01.011

Denich, C., Bradford, A., Drake, J., 2013. Bioretention: assessing effects of winter salt and aggregate application on plant health, media clogging and effluent quality. Water Qual. Res. J. 48, 387–399. https://doi.org/10.2166/wqrjc.2013.065

Ding, B., Rezanezhad, F., Gharedaghloo, B., Van Cappellen, P., Passeport, E., 2019. Bioretention cells under cold climate conditions: Effects of freezing and thawing on water infiltration, soil structure, and nutrient removal. Sci. Total Environ. 649, 749–759. https://doi.org/10.1016/j.scitotenv.2018.08.366

Géhéniau, N., Fuamba, M., Mahaut, V., Gendron, M.R., Dugué, M., 2015. Monitoring of a rain garden in cold climate: Case study of a parking lot near Montréal. J. Irrig. Drain. Eng. 141. https://doi.org/10.1061/(ASCE)IR.1943-4774.0000836

Glaister, B.J., Fletcher, T.D., Cook, P.L.M., Hatt, B.E., 2014. Co-optimisation of phosphorus and nitrogen removal in stormwater biofilters: the role of filter media, vegetation and saturated zone. Water Sci. Technol. 69, 1961–1969. https://doi.org/10.2166/wst.2014.117

Goor, J., Cantelon, J., Smart, C., Robinson, C.E., 2021. Seasonal performance of field bioretention systems in retaining phosphorus in a cold climate: Influence of prolonged road salt application. Sci. Total Environ. 146069. https://doi.org/10.1016/j.scitotenv.2021.146069

Gregory, C., Goltz, D., Kumaragamage, D., Singh, J., Indraratne, S., 2017. Comparison of phosphorus release to pore water and floodwater from Manitoba soils under simulated spring snowmelt and simulated summer flooding conditions, in: Proceedings of the Canadian Soil Science Society Annual Meetings. Peterborough, ON.

Guardado, I., Urrutia, O., García-Mina, J.M., 2007. Size Distribution, Complexing Capacity, and Stability of Phosphate−Metal−Humic Complexes. J. Agric. Food Chem. 55, 408–413. https://doi.org/10.1021/jf062894y

Guo, C., Li, J., Li, H., Li, Y., 2019. Influences of stormwater concentration infiltration on soil nitrogen, phosphorus, TOC and their relations with enzyme activity in rain garden. Chemosphere 233, 207–215. https://doi.org/10.1016/j.chemosphere.2019.05.236

Helsel, D.R., 2011. Statistics for Censored Environmental Data Using Minitab® and R, 2nd ed. John Wiley & Sons, Inc., Hoboken, NJ, USA. https://doi.org/10.1002/9781118162729

Helsel, D.R., Hirsch, R.M., Ryberg, K.R., Archfield, S.A., Gilroy, E.J., 2020. Statistical methods in water resources, Techniques and Methods. Reston, VA. https://doi.org/10.3133/tm4A3

Hobbie, S.E., Finlay, J.C., Janke, B.D., Nidzgorski, D.A., Millet, D.B., Baker, L.A., 2017. Contrasting nitrogen and phosphorus budgets in urban watersheds and implications for managing urban water pollution. Proc. Natl. Acad. Sci. 114, 4177–4182. https://doi.org/10.1073/pnas.1618536114

Hsieh, C., Davis, A.P., Needelman, B.A., 2007. Bioretention Column Studies of Phosphorus Removal from Urban Stormwater Runoff. Water Environ. Res. 79, 177–184. https://doi.org/10.2175/106143006x111745

Hunt, W.F., Jarrett, A.R., Smith, J.T., Sharkey, L.J., 2006a. Evaluating bioretention hydrology and nutrient removal at three field sites in North Carolina. J. Irrig. Drain. Eng. 132, 600–608. https://doi.org/10.1061/(ASCE)0733-9437(2006)132:6(600)

Hunt, W.F., Jarrett, A.R., Smith, J.T., Sharkey, L.J., 2006b. Evaluating bioretention hydrology and nutrient removal at three field sites in North Carolina. J. Irrig. Drain. Eng. 132, 600–608. https://doi.org/10.1061/(ASCE)0733-9437(2006)132:6(600)

Janke, B.D., Finlay, J.C., Hobbie, S.E., 2017. Trees and Streets as Drivers of Urban Stormwater Nutrient Pollution. Environ. Sci. Technol. 51, 9569–9579. https://doi.org/10.1021/acs.est.7b02225

Johnson, J.P., Hunt, W.F., 2020. Field Assessment of the Hydrologic Mitigation Performance of Three Aging Bioretention Cells. J. Sustain. Water Built Environ. 6, 04020017. https://doi.org/10.1061/jswbay.0000925

Johnson, J.P., Hunt, W.F., 2019. A retrospective comparison of water quality treatment in a bioretention cell 16 years following initial analysis. Sustain. Switz. 11, 1945. https://doi.org/10.3390/su11071945

Johnson, J.P., Hunt, W.F., 2016. Evaluating the spatial distribution of pollutants and associated maintenance requirements in an 11 year-old bioretention cell in urban Charlotte, NC. J. Environ. Manage. 184, 363–370. https://doi.org/10.1016/j.jenvman.2016.10.009

Kandel, S., 2016. Phosphorus and metal sorption in aged bioretention cells with fly-ash amended filter media. Oklahoma State University.

Kandel, S., Vogel, J., Penn, C., Brown, G., 2017. Phosphorus Retention by Fly Ash Amended Filter Media in Aged Bioretention Cells. Water 9, 746. https://doi.org/10.3390/w9100746

Kleinman, P.J.A., Sharpley, A.N., Gartley, K., Jarrell, W.M., Kuo, S., Menon, R.G., Myers, R., Reddy, K.R., Skogley, E.O., 2007. Interlaboratory comparison of soil phosphorus extracted by various soil test methods. Httpdxdoiorg101081CSS-120000376 32, 2325–2345. https://doi.org/10.1081/CSS-120000376

Komlos, J., Traver, R.G., 2012. Long-Term Orthophosphate Removal in a Field-Scale Storm-Water Bioinfiltration Rain Garden. J. Environ. Eng. 138, 991–998. https://doi.org/10.1061/(ASCE)EE.1943-7870.0000566

Lammers, R.W., Bledsoe, B.P., 2017. What role does stream restoration play in nutrient management? Crit. Rev. Environ. Sci. Technol. 47, 335–371. https://doi.org/10.1080/10643389.2017.1318618

Li, H., Davis, A.P., 2008a. Urban Particle Capture in Bioretention Media. II: Theory and Model Development. J. Environ. Eng. 134, 419–432. https://doi.org/10.1061/(asce)0733-9372(2008)134:6(419)

Li, H., Davis, A.P., 2008b. Urban Particle Capture in Bioretention Media. I: Laboratory and Field Studies. J. Environ. Eng. 134, 409–418. https://doi.org/10.1061/(asce)0733-9372(2008)134:6(409)

Li, J., Davis, A.P., 2016a. A unified look at phosphorus treatment using bioretention. Water Res. 90, 141–155. https://doi.org/10.1016/j.watres.2015.12.015

Li, J., Davis, A.P., 2016b. A unified look at phosphorus treatment using bioretention. Water Res. 90, 141–155. https://doi.org/10.1016/j.watres.2015.12.015

Li, J., Zhao, R., Li, Y., Chen, L., 2018. Modeling the effects of parameter optimization on three bioretention tanks using the HYDRUS-1D model. J. Environ. Manage. 217, 38–46. https://doi.org/10.1016/j.jenvman.2018.03.078

Li, Y., Fu, H., Zhang, J., Zhang, Z., Li, J., 2021. Study of pollutant accumulation characteristics and microbial community impact at three bioretention facilities. Environ. Sci. Pollut. Res. 28, 44389–44407. https://doi.org/10.1007/s11356-021-13801-0

Liu, J., Davis, A.P., 2014. Phosphorus speciation and treatment using enhanced phosphorus removal bioretention. Environ. Sci. Technol. 48, 607–614. https://doi.org/10.1021/es404022b

Liu, Y., Goor, J., Robinson, C.E., 2021. Behaviour of soluble reactive phosphorus within field-scale bioretention systems. J. Hydrol. 601, 126597. https://doi.org/10.1016/j.jhydrol.2021.126597

Lucke, T., Nichols, P.W.B.B., 2015. The pollution removal and stormwater reduction performance of street-side bioretention basins after ten years in operation. Sci. Total Environ. https://doi.org/10.1016/j.scitotenv.2015.07.142

Luo, H., Guan, L., Jing, Z., He, B., Cao, X., Zhang, Z., Tao, M., 2020. Performance evaluation of enhanced bioretention systems in removing dissolved nutrients in stormwater runoff. Appl. Sci. 10, 3148. https://doi.org/10.3390/app10093148

Manka, B.N., Hathaway, J.M., Tirpak, R.A., He, Q., Hunt, W.F., 2016. Driving forces of effluent nutrient variability in field scale bioretention. Ecol. Eng. https://doi.org/10.1016/j.ecoleng.2016.06.024

Marvin, J.T., Passeport, E., Drake, J., 2020. State-of-the-Art Review of Phosphorus Sorption Amendments in Bioretention Media: A Systematic Literature Review. J. Sustain. Water Built Environ. 6, 03119001. https://doi.org/10.1061/JSWBAY.0000893

McManus, M., Davis, A.P., 2020. Impact of Periodic High Concentrations of Salt on Bioretention Water Quality Performance. J. Sustain. Water Built Environ. 6. https://doi.org/10.1061/JSWBAY.0000922

Miguntanna, N.P., Liu, A., Egodawatta, P., Goonetilleke, A., 2013. Characterising nutrients wash-off for effective urban stormwater treatment design. J. Environ. Manage. 120, 61–67. https://doi.org/10.1016/j.jenvman.2013.02.027

Muerdter, C., Özkök, E., Li, L., Davis, A.P., 2016. Vegetation and media characteristics of an effective bioretention cell. J. Sustain. Water Built Environ. 2, 04015008. https://doi.org/10.1061/JSWBAY.0000804

O'Connell, D.W., Ansems, N., Kukkadapu, R.K., Jaisi, D., Orihel, D.M., Cade-Menun, B.J., Hu, Y., Wiklund, J., Hall, R.I., Chessell, H., Behrends, T., Van Cappellen, P., 2020. Changes in Sedimentary Phosphorus Burial Following Artificial Eutrophication of Lake 227, Experimental Lakes Area, Ontario, Canada. J. Geophys. Res. Biogeosciences 125, e2020JG005713. https://doi.org/10.1029/2020JG005713

Oksanen, J., Blanchet, F.G., Friendly, M., Kindt, R., Legendre, P., McGlinn, D., Minchin, P.R., O'Hara, R.B., Simpson, G.L., Solymos, P., Stevens, M.H.H., Szoecs, E., Wagner, H., 2020. vegan: Community Ecology Package.

Pallud, C., Van Cappellen, P., 2006. Kinetics of microbial sulfate reduction in estuarine sediments. Geochim. Cosmochim. Acta 70, 1148–1162. https://doi.org/10.1016/j.gca.2005.11.002

Parsons, C.T., Rezanezhad, F., O'Connell, D.W., Van Cappellen, P., 2017. Sediment phosphorus speciation and mobility under dynamic redox conditions. Biogeosciences 14, 3585–3602. https://doi.org/10.5194/bg-14-3585-2017

Poikane, S., Kelly, M.G., Salas Herrero, F., Pitt, J.-A., Jarvie, H.P., Claussen, U., Leujak, W., Lyche Solheim, A., Teixeira, H., Phillips, G., 2019. Nutrient criteria for surface waters under the European Water Framework Directive: Current state-of-the-art, challenges and future outlook. Sci. Total Environ. 695, 133888. https://doi.org/10.1016/j.scitotenv.2019.133888

Radosavljevic, J., Slowinski, S., Shafii, M., Akbarzadeh, Z., Rezanezhad, F., Parsons, C.T., Withers, W., Van Cappellen, P., 2022. Salinization as a driver of eutrophication symptoms in an urban lake (Lake Wilcox, Ontario, Canada). Sci. Total Environ. 846, 157336. https://doi.org/10.1016/j.scitotenv.2022.157336

Roy-Poirier, A., Champagne, P., Filion, Y., 2010. Review of bioretention system research and design: past, present, and future. J. Environ. Eng. 136, 878–889. https://doi.org/10.1061/(ASCE)EE.1943-7870.0000227

Ruttenberg, K.C., 1992. Development of a sequential extraction method for different forms of phosphorus in marine sediments. Limnol. Oceanogr. 37, 1460–1482. https://doi.org/10.4319/lo.1992.37.7.1460

Ruttenberg, K.C., Ogawa, N.O., Tamburini, F., Briggs, R.A., Colasacco, N.D., Joyce, E., 2009. Improved, high-throughput approach for phosphorus speciation in natural sediments via the SEDEX sequential extraction method. Limnol. Oceanogr. Methods 7, 319–333. https://doi.org/10.4319/lom.2009.7.319

Sansalone, J.J., Buchberger, S.G., 1996. Characterization of Metals and Solids in Urban Highway Winter Snow and Spring Rainfall-Runoff. Transp. Res. Rec. J. Transp. Res. Board 1523, 147–159. https://doi.org/10.1177/0361198196152300118

Shetterly, B.J., 2018. Soil phosphorus characterization and vulnerability to release in urban stormwater bioretention facilities. Portland State University.

Smyth, K., Drake, J., Li, Y., Rochman, C., Van Seters, T., Passeport, E., 2021. Bioretention cells remove microplastics from urban stormwater. Water Res. 191, 116785. https://doi.org/10.1016/j.watres.2020.116785

Song, K., Xenopoulos, M.A., Marsalek, J., Frost, P.C., 2015. The fingerprints of urban nutrients: dynamics of phosphorus speciation in water flowing through developed landscapes. Biogeochemistry 125. https://doi.org/10.1007/s10533-015-0114-3

Song, Y., Song, S., 2019. Migration and transformation of different phosphorus forms in rainfall runoff in bioretention system. Environ. Sci. Pollut. Res. 26, 30633–30640. https://doi.org/10.1007/s11356-018-2405-4

Spivakov, B.Y.A., Maryutina, T.A., Muntau, H., 1999. Phosphorus speciation in water and sediments (Technical Report). Pure Appl. Chem. 71, 2161–2176. https://doi.org/10.1351/pac199971112161

Spraakman, S., 2021. Bioretention Systems for Stormwater Management: Assessment, Performance and Changes Over Time. University of Toronto, Toronto.

Spraakman, S., Rodgers, T.F.M., Monri-Fung, H., Nowicki, A., Diamond, M.L., Passeport, E., Thuna, M., Drake, J., 2020. A Need for Standardized Reporting: A Scoping Review of Bioretention Research 2000–2019. Water 12, 3122. https://doi.org/10.3390/w12113122

US EPA, 2022. State-Specific Water Quality Standards Effective under the Clean Water Act (CWA) [WWW Document]. State-Specif. Water Qual. Stand. Eff. Clean Water Act CWA. URL https://www.epa.gov/wqs-tech/state-specific-water-quality-standards-effective-under-clean-water-act-cwa (accessed 7.29.22).

US EPA, 2007. Method 6010C (SW-846): Inductively Coupled Plasma-Atomic Emission Spectrometry,.

US EPA, 1986. Quality Criteria For Water, Gold Book. ed. United States Environment Protection Agency.

US EPA, O., 2019. EPA Method 3050B: Acid Digestion of Sediments, Sludges, and Soils. United States Environment Protection Agency.

Willard, L.L., Wynn-Thompson, T., Krometis, L.H., Neher, T.P., Badgley, B.D., 2017. Does It Pay to be Mature? Evaluation of Bioretention Cell Performance Seven Years Postconstruction. J. Environ. Eng. 143, 04017041. https://doi.org/10.1061/(asce)ee.1943-7870.0001232

Yan, Q., James, B.R., Davis, A.P., 2017. Lab-scale column studies for enhanced phosphorus sorption from synthetic urban stormwater using modified bioretention media. J. Environ. Eng. 143, 04016073. https://doi.org/10.1061/(ASCE)EE.1943-7870.0001159

Yang, Y.-Y., Lusk, M.G., 2018. Nutrients in Urban Stormwater Runoff: Current State of the Science and Potential Mitigation Options. Curr. Pollut. Rep. 4, 112–127. https://doi.org/10.1007/s40726-018-0087-7

Yu, G., Zhang, B., Lu, X., Li, J., Chen, J., Zuo, J., 2015. Efficient removal of phosphorus in bioretention system by sludge pyrolysis residue. Arab. J. Geosci. 8, 3491–3499. https://doi.org/10.1007/s12517-014-1462-3

Zhang, B., Li, J., Li, Y., Li, H., 2018. Adsorption characteristics of several bioretention-modified fillers for phosphorus. Water 10, 831. https://doi.org/10.3390/w10070831

Zhang, Z., Li, J., Li, Y., Wang, D., Zhang, J., Zhao, L., 2021. Assessment on the cumulative effect of pollutants and the evolution of micro-ecosystems in bioretention systems with different media. Ecotoxicol. Environ. Saf. 228, 112957. https://doi.org/10.1016/j.ecoenv.2021.112957

APPENDICES

A1. Summary of Analyses Performed

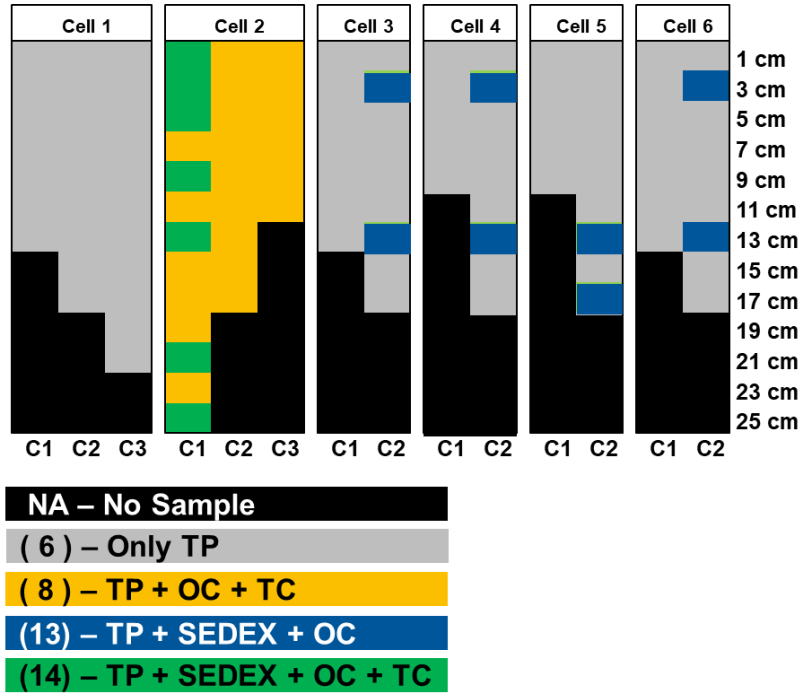

a

Figure A1-1: Colour coded summary of the tests performed on each of the slices available. TP, OC, TC and SEDEX represent total phosphorus (Aspila et al 1976), Organic Carbon, Total Carbon (Elementar vario EL cube) and SEDEX methods (Modified from Ruttenberg et al. 1992)

A2. Result value heatmaps

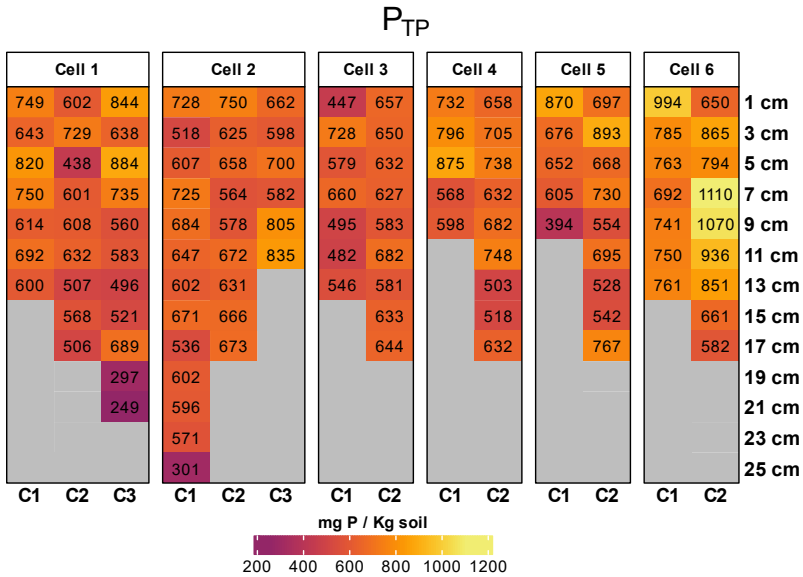

Figure A2-1: Summary heatmap of TP concentrations in all samples. A total of 115 different samples were analyzed of which 0 were below the detection limit (indicated with a '<'). Asterisks show samples that were available but not measured,

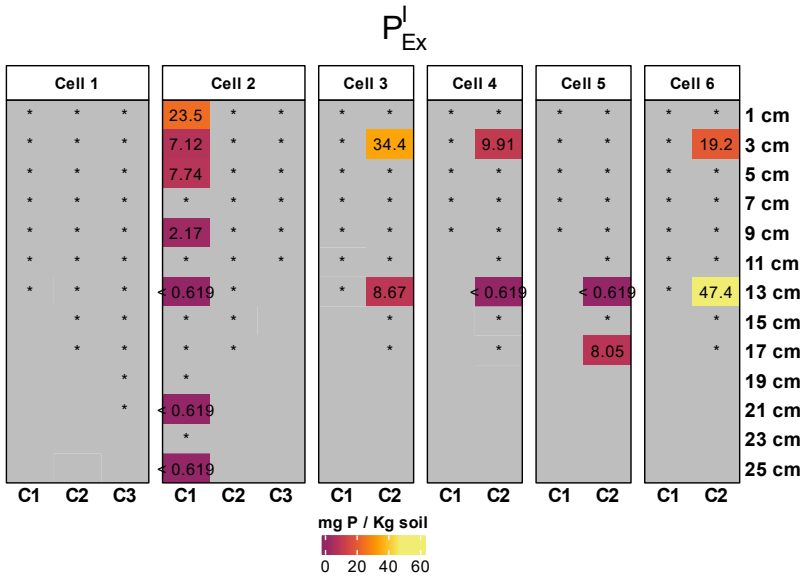

Figure A2-2: Summary heatmap of $\boldsymbol{P^{I}_{Ex}}$concentrations in all samples. A total of 15 different samples were analyzed of which 5 were below the detection limit (indicated with a '<'). Asterisks show samples that were available but not measured,

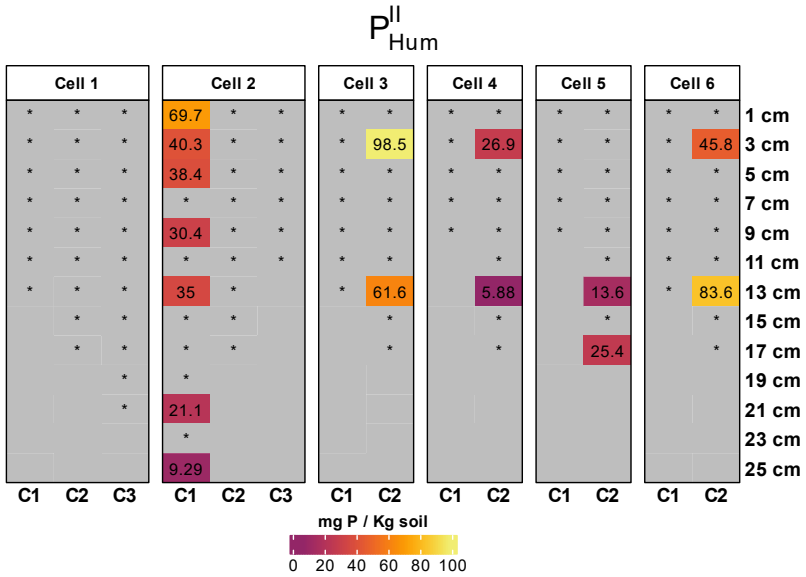

Figure A2-3: Summary heatmap of $\boldsymbol{P^{II}_{Hum}}$ concentrations in all samples. A total of 15 different samples were analyzed of which 0 were below the detection limit (indicated with a '<'). Asterisks show samples that were available but not measured,

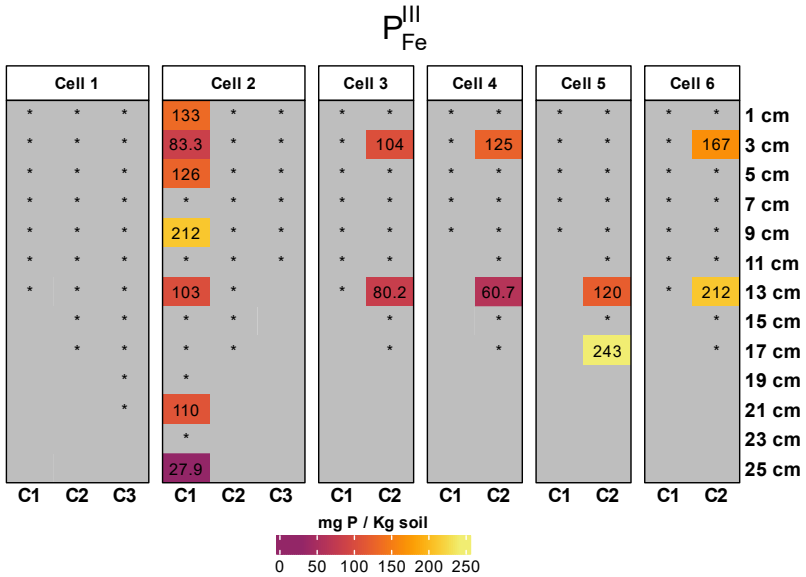

Figure A2-4: Summary heatmap of $\mathbf{P^{III}_{Fe}}$ concentrations in all samples. A total of 15 different samples were analyzed of which 0 were below the detection limit (indicated with a '<'). Asterisks show samples that were available but not measured,

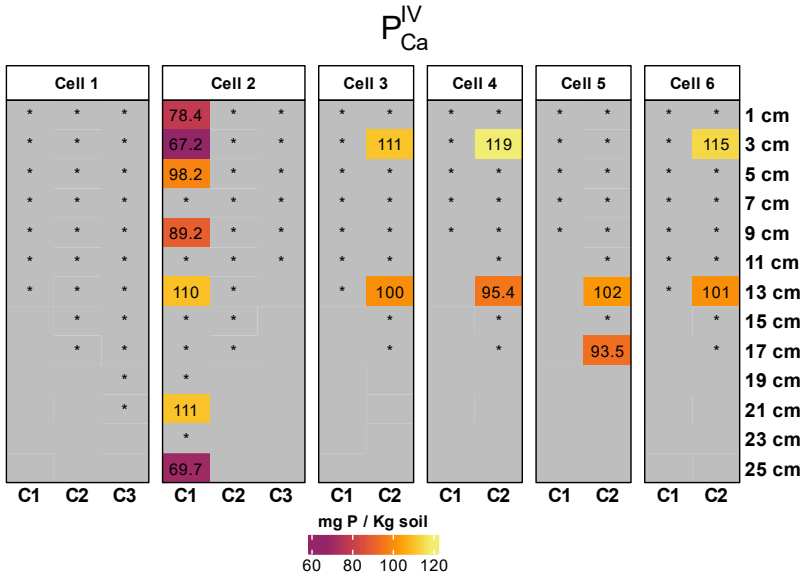

Figure A2-5: Summary heatmap of $\mathbf{P^{IV}_{Ca}}$ concentrations in all samples. A total of 15 different samples were analyzed of which 0 were below the detection limit (indicated with a '<'). Asterisks show samples that were available but not measured.

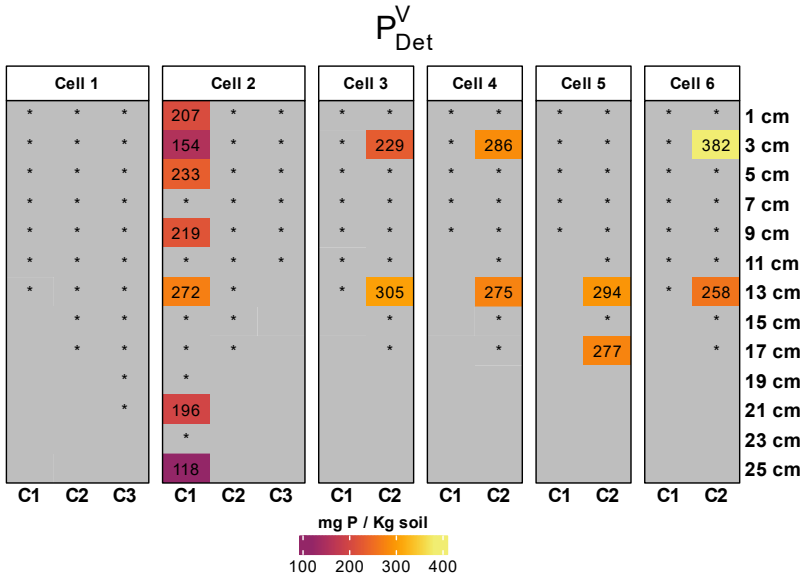

Figure A2-6: Summary heatmap of $\mathbf{P^{V}_{Det}}$ concentrations in all samples. A total of 15 different samples were analyzed of which 0 were below the detection limit (indicated with a '<'). Asterisks show samples that were available but not measured.

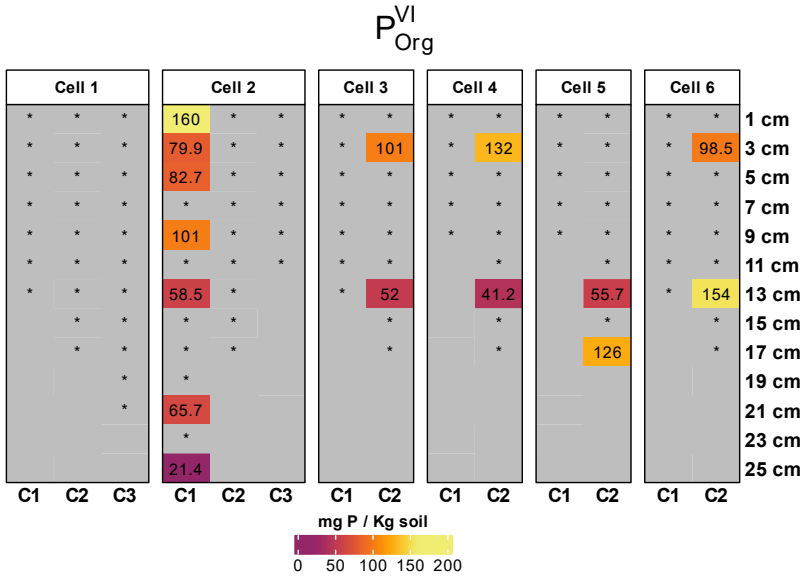

Figure A2-7: Summary heatmap of $\mathbf{P^{VI}_{Org}}$ concentrations in all samples. A total of 15 different samples were analyzed of which 0 were below the detection limit (indicated with a '<'). Asterisks show samples that were available but not measured.

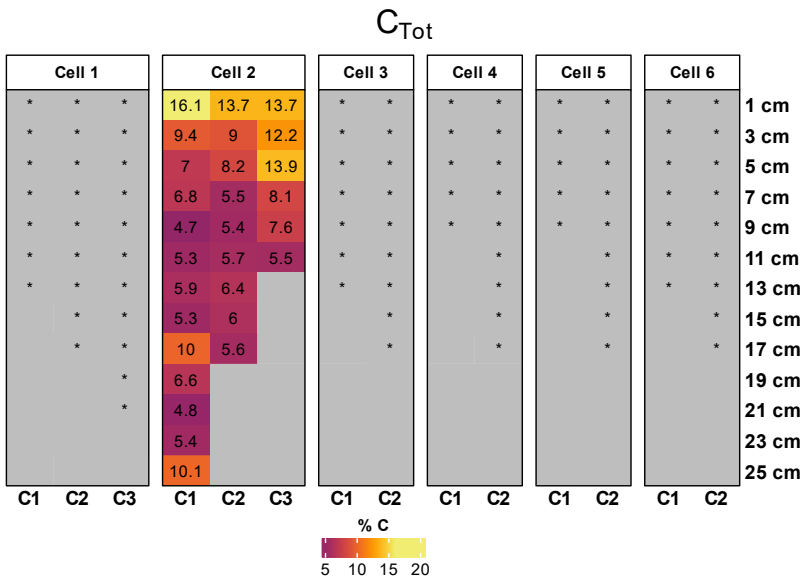

Figure A2-8: Summary heatmap of TC concentrations in all samples. A total of 28 different samples were analyzed of which 0 were below the detection limit (indicated with a '<'). Asterisks show samples that were available but not measured.

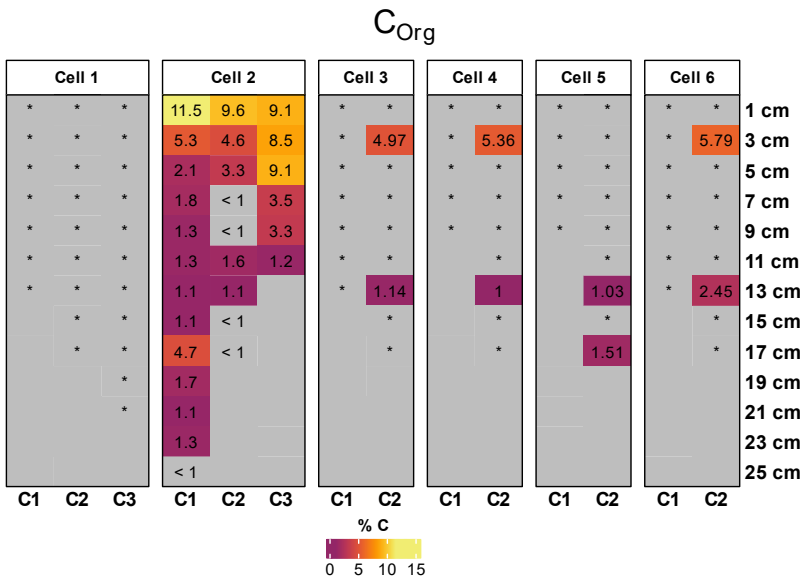

Figure A2-9: Summary heatmap of OC concentrations in all samples. A total of 36 different samples were analyzed of which 5 were below the detection limit (indicated with a '<'). Asterisks show samples that were available but not measured.

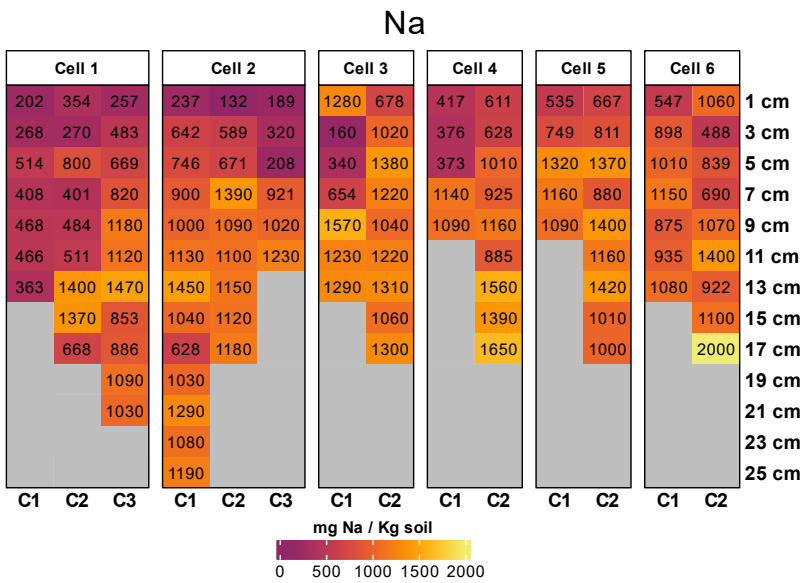

Figure A2-10: Summary heatmap of Na concentrations in all samples. A total of 115 different samples were analyzed.

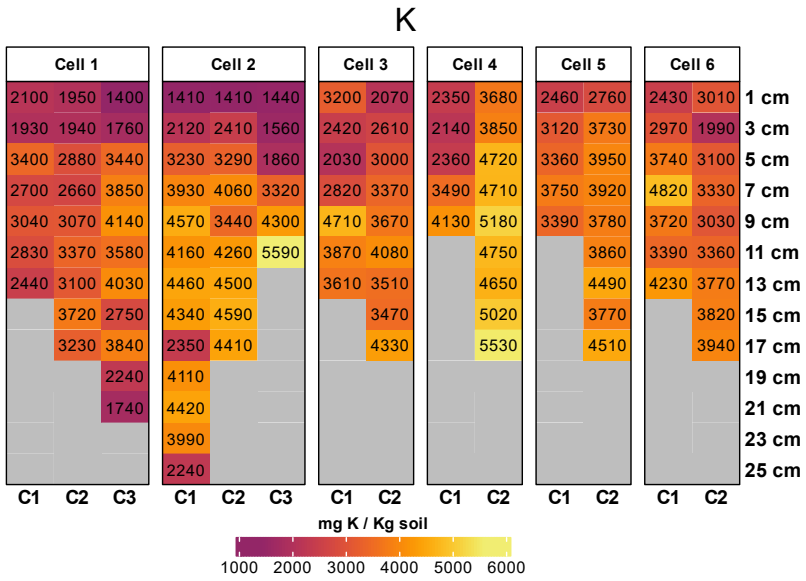

Figure A2-11: Summary heatmap of K concentrations in all samples A total of 115 different samples were analyzed.

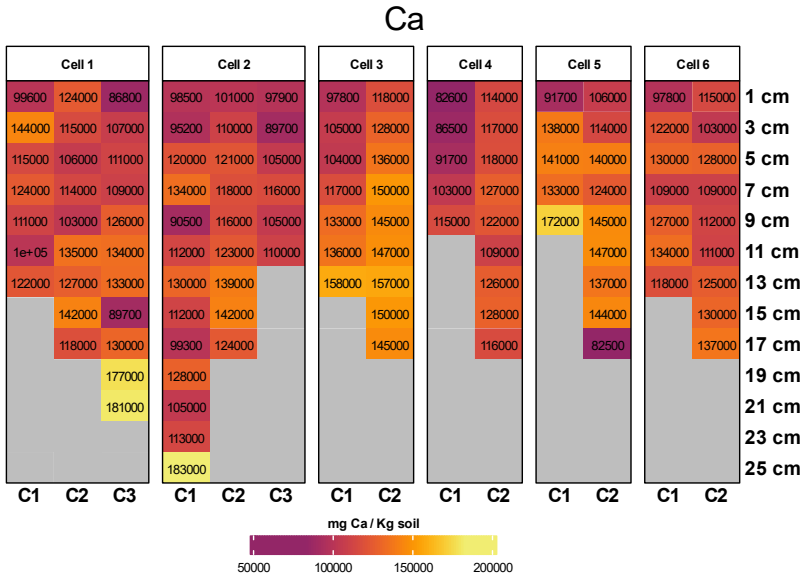

Figure A2-12: A total of 115 different samples were analyzed.

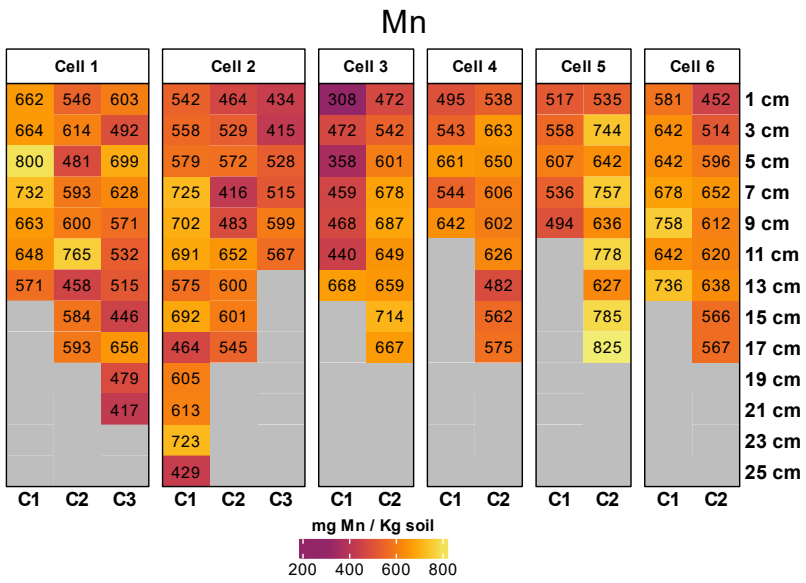

Figure A2-13: A total of 115 different samples were analyzed.

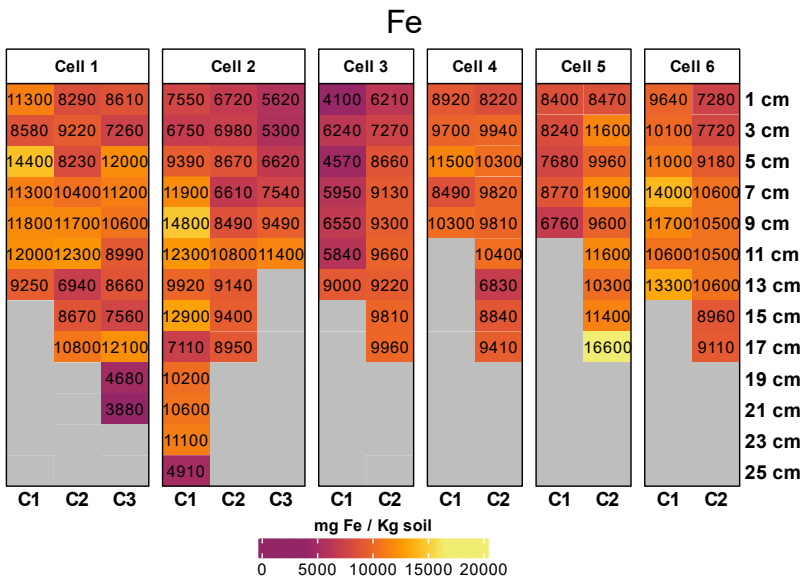

Figure A2-14: A total of 115 different samples were analyzed.

A3. Temporal changes of other filtration media parameters in CVC Technical Report

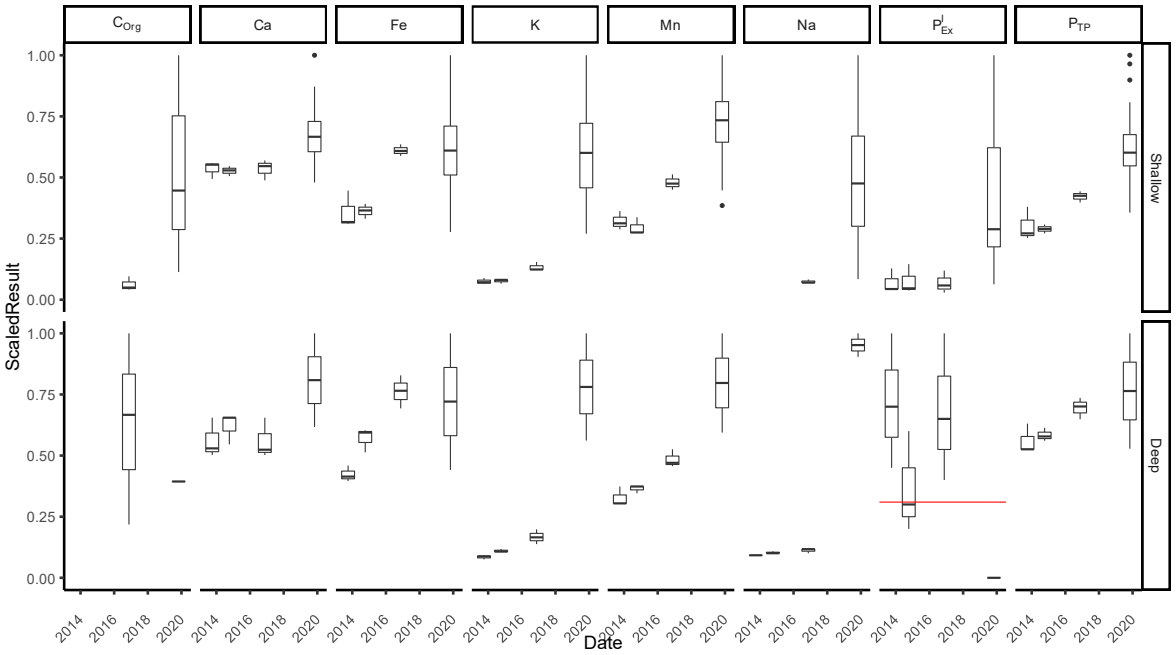

Figure A3-1: Distribution of results for the parameters analyzed in this study compared to equivalent measurements present in previously published (CVC 2016) dataset for the site. A red horizontal line was used to identify the maximum threshold for non-detects in the cases where other measurements were reported uncensored below it for that parameter. Separation of shallow (< 10) deep (> 23 cm) measurements is discussed further in the article.

A4. Differences between our methods and CVC reports

We used the acid extractable metal concentrations (Na, K, Ca, Mn and Fe) reported with the TP method (SW-846-6010C) and "Total Organic Carbon" (only reported in 2016 using "BCMOE TOC Aug 2014" method) to compare with our own values (acquired with methods discussed in the manuscript). Though not directly comparable, both approximate the total available content within the soil.

A5. Correlograms for all parameters measured in 2019

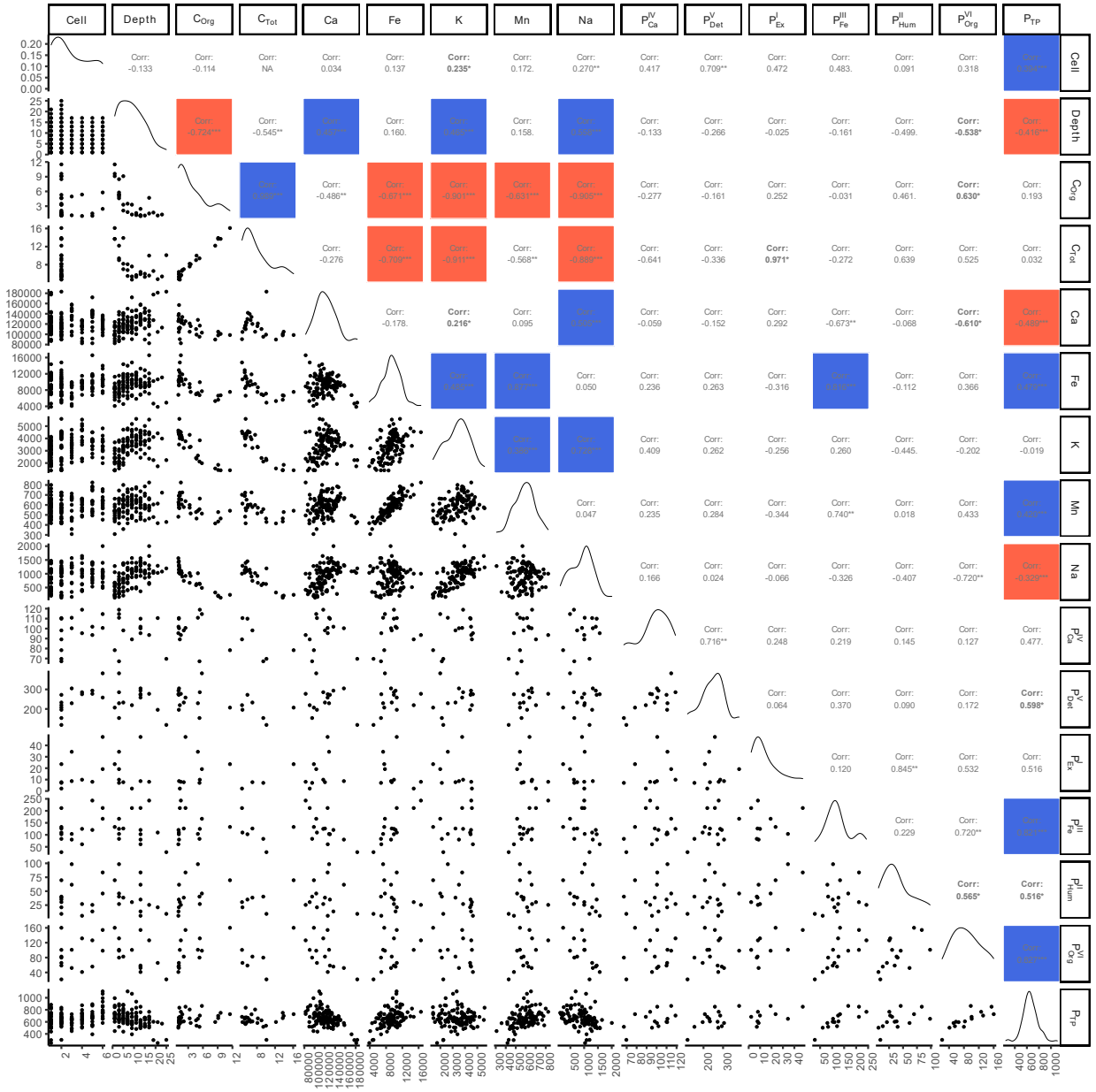

Figure A5-1: Pairwise (Pearson) correllogram of all parameters in dataset. Values below detection limits omitted. Pearson correlation coefficients shown between pairs of parameters and significance (p=0.05, p=0.01 and p=0.001 as * , ** , and *** respectively)

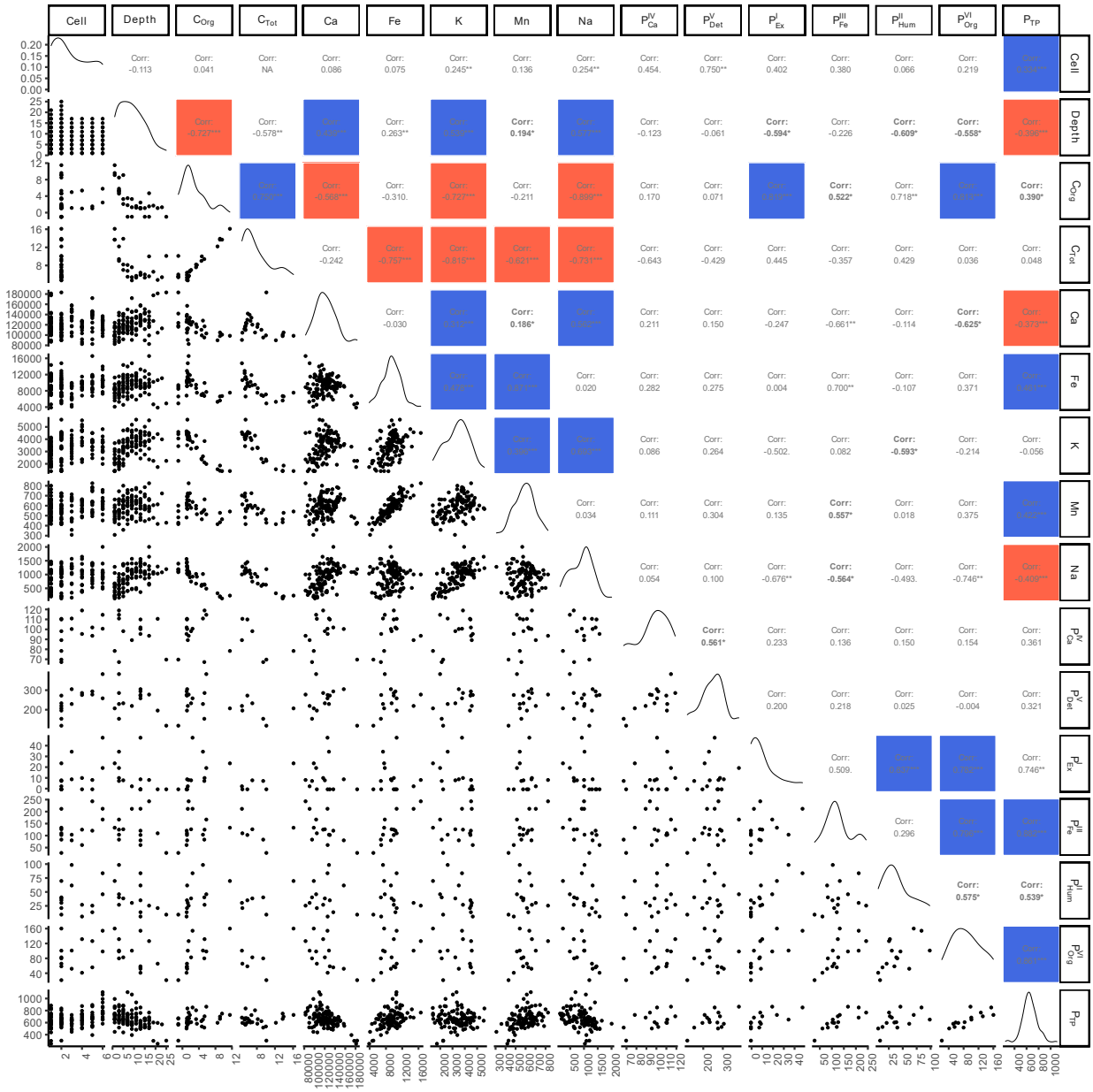

Figure A5-2: Pairwise (Spearman) correllogram of all parameters in dataset. Values below detection limits ranked as minimum Spearman correlation coefficients shown between pairs of parameters and significance (p=0.05, p=0.01 and p=0.001 as * , ** , and *** respectively).

A6. Fractional P content of all SEDEX samples

Table A6-1 Concentrations of individual P fractions of each sample measured using the SEDEX method. Proportions relative to TP measured in the same samples (using a separate method) shown as percentages. Sum of all SEDEX fractional concentrations indicated as `**Σ** SEDEX`.

Cell	Core	Depth cm	P^{I}_{Ex} mgP kg^{-1}	P^{II}_{Hum} mgP kg^{-1}	P^{III}_{Fe} mgP kg^{-1}	P^{IV}_{Ca} mgP kg^{-1}	P^{V}_{Det} mgP kg^{-1}	P^{VI}_{Org} mgP kg^{-1}	Σ SEDEX
2	**1**	**1**	23.5 (%3.23)	69.7 (%9.57)	133 (%18.3)	78.4 (%10.8)	207 (%28.4)	160 (%22)	671 (%92.2)
		3	7.12 (%1.38)	40.3 (%7.78)	83.3 (%16.1)	67.2 (%13)	154 (%29.7)	79.9 (%15.4)	431 (%83.3)
		5	7.74 (%1.27)	38.4 (%6.32)	126 (%20.8)	98.2 (%16.2)	233 (%38.3)	82.7 (%13.6)	586 (%96.5)
		9	2.17 (%0.317)	30.4 (%4.44)	212 (%30.9)	89.2 (%13)	219 (%32.1)	101 (%14.7)	653 (%95.5)
		13	<	35 (%5.82)	103 (%17)	110 (%18.3)	272 (%45.2)	58.5 (%9.73)	578 (%96.1)
		21	<	21.1 (%3.54)	110 (%18.4)	111 (%18.6)	196 (%32.9)	65.7 (%11)	503 (%84.4)
		25	<	9.29 (%3.08)	27.9 (%9.25)	69.7 (%23.1)	118 (%39.3)	21.4 (%7.09)	247 (%81.8)
3	**2**	**3**	34.4 (%5.28)	98.5 (%15.1)	104 (%15.9)	111 (%17)	229 (%35.2)	101 (%15.5)	678 (%104)
		13	8.67 (%1.49)	61.6 (%10.6)	80.2 (%13.8)	100 (%17.3)	305 (%52.5)	52 (%8.96)	608 (%105)
4	**2**	**3**	9.91 (%1.41)	26.9 (%3.82)	125 (%17.7)	119 (%16.9)	286 (%40.5)	132 (%18.7)	698 (%99)
		13	<	5.88 (%1.17)	60.7 (%12.1)	95.4 (%19)	275 (%54.8)	41.2 (%8.2)	478 (%95.2)
5	**2**	**13**	<	13.6 (%2.58)	120 (%22.8)	102 (%19.3)	294 (%55.6)	55.7 (%10.6)	585 (%111)
		17	8.05 (%1.05)	25.4 (%3.31)	243 (%31.7)	93.5 (%12.2)	277 (%36.2)	126 (%16.5)	774 (%101)
6	**2**	**3**	19.2 (%2.22)	45.8 (%5.3)	167 (%19.3)	115 (%13.3)	382 (%44.2)	98.5 (%11.4)	827 (%95.7)
		13	47.4 (%5.57)	83.6 (%9.82)	212 (%24.9)	101 (%11.8)	258 (%30.3)	154 (%18.1)	856 (%101)

A7. Bioretention cells models in literature mentioning accumulation

DOI	Year of Publication	Authors	Model Name	Model Scale	Data Source	Black Box (Only In/Out ratios)	Measured	Reported	Represented in Model	Model (soil) Results presented	Notes
https://doi.org/10.1080/01426397.2018.1498071	2019	Pierre, A., Amoroso, N. and Kelly, S.	CityEngine	Catchment	Single case study - Industrial	-	-	-	-	-	Single, non peer-reviewed source used for ratio estimations
https://doi.org/10.1016/j.jenvman.2018.03.078	2018	Li, Jiake, Zhao, Ruisong, Li, Yajiao and Chen, Li	HYDRUS-1D	Bioretention		*	-	-	*	-	Despite being mentioned, the soil terms are excluded for simplificatoin
https://doi.org/10.1016/j.jenvman.2014.09.005	2015	Liu, Y. Z., Ahiablame, L. M., Bralts, V. F. and Engel, B. A.	L-THIA	Catchment	BMP Database	x	-	-	-	-	Unclear model operation/parameters, Literature cited (DOI: 10.5539/ep.v1n2p1) only mentions empirical approach to water quantity, Liu et al (2018) mention it's a fixed percent
https://doi.org/10.1016/j.watres.2015.12.015	2016	Li, Jiake and Davis, Allen P.	Li & Davis (2016)	Bioretention	Laboratory Studies - Columns	/	-	-	*	-	Soil related parameters in equations listed for primary parameter modelled (Ceq)
https://doi.org/10.1016/j.jhydrol.2018.03.053	2018	Yaoze, Liu, Engel, B. A., Flanagan, D. C., Gitau, M. W., McMillan, S. K., Chaubey, I. and Singh, S.	Liu 2018	Bioretention	BMP Database	x	-	-	-	-	Broad framework, uses same database as prior
https://doi.org/10.1061/(ASCE)EE.1943-7870.0001526	2019	Xu, X. and Zhang, Q.	Lynn (2014)	Bioretention		-	-	**	?	**	Model mentions P processes near surface but does not provide equations, suggests P removal by surface plants and quantifies media export quantities.
https://dx.doi.org/10.1504/IJW.2015.070362	2015	Imteaz, Monzur A. and Ahsan, Amimul	MUSIC	Bioretention; catchment		x	-	-	-	-	

https://doi.org/10.1016/j.resconrec.2012.11.007	2013	Imteaz, M. A., Ahsan, A., Rahman, A. and Mekanik, F.	MUSIC	Catchment	Unclear	x	-	-	-	-	MUSIC had poor performance modelling TP, only reduction percentages (concentration)
http://dx.doi.org/10.1504/IJESD.2016.073333	2016	Rahman, M. A., Imteaz, M. A. and Arulrajah, A.	MUSIC	Bioretention		x	-	-	-	-	No P accumulation measured in soil.
https://doi.org/10.5004/dwt.2019.24684	2019	Gulbaz, S.	SWMM	Catchment; bioretention		x	-	-	-	-	
https://doi.org/10.1007/s11356-019-04129-x	2019	Wang, H. W., Zhai, Y. J., Wei, Y. Y. and Mao, Y. F.	SWMM	Catchment; bioretention		x	-	-	?	-	model does not include P, unclear units for reduction, SUSTAIN is an extension of SWMM by EPA which
https://doi.org/10.1016/j.ecoleng.2011.01.008	2011	Hurley, Stephanie E. and Forman, Richard T. T.	WinSLAMM	Catchment	Own Field Study	x	-	-	-	-	Model calculates particulate filtration but no accumulation in soil nor any partitioning thereafter.
https://doi.org/10.1016/j.jhydrol.2021.126597	2021	Liu, Y., Goor, J., & Robinson, C. E.	PHREEQC	Process/pore water	Own Field Study	-	x	x	x	x	PHREEQC was used to estimate partitioning to certain P minerals, Only soluble fraction and unestablished cells were assessed

x present in study || - missing
* Partially represented, used equilibrium with water instead
? Model mentioned includes process-based modelling with some soil processes though they're not explicitly mentioned or elaborated upon.
/ Other studies showing soil accumulation rates and patterns discussed.
** Reports values for overall media export, full source unclear

A8. Image of extraction manifolds used for SEDEX procedure

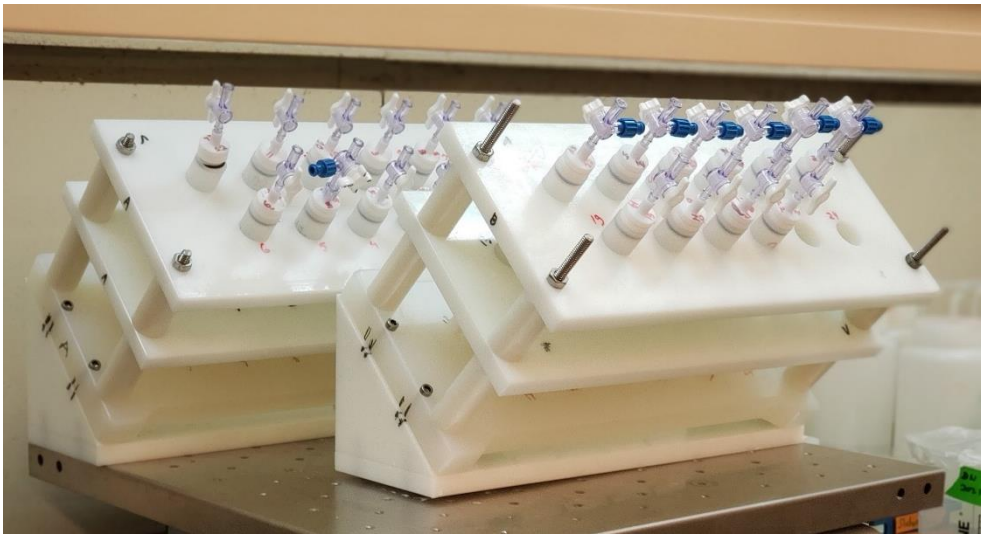

Figure A8-3: Image of extraction manifolds used for SEDEX procedure. Two manifolds containing filter me

A9. Quality Assurance Procedures

Both TP extraction and SEDEX procedures included various quality control and assurance steps. For the TP procedure, at least one method blank and two reference materials (of which at least one was externally certified) were included in each batch of samples during digestion and extraction steps. European Commission Community Bureau of Reference BCR Reference Material No. 684 "River Sediment (Extractable Phosphorous)" was used as our external reference material. A subsample of the reference material was taken at the start of the analysis process and subjected to the same storage conditions as the filter media samples throughout the analytical procedure. All results for the reference material were within the 95% confidence interval of the certified "Conc. HCl-extract. P value" value reported. Repeated analyses of both the external and internal reference materials used were consistently produced results within 3% of the mean value determined from all measurements in different runs. Method blank samples, included with every batch were treated identically to those containing media for analysis including the $MgNO_3$ addition, digestion, re-suspension, and extraction steps to identify whether any potential contamination may have occurred within them. None of the concentrations reported in the method blanks were significantly different than those in the matrix-matched instrument blanks (discussed below).

For the SEDEX procedure, each run of samples was performed in duplicate and included (duplicate) blank, externally sourced and internally sourced reference materials. As no certified reference material that provided a good match for intermediate SEDEX fractional concentrations was available. Regardless, the sum of all SEDEX fractions in both of the runs for which data is shown was within 3% of the certified "Conc. HCl-extract. P value" in both of the SEDEX runs performed.

For ICP-OES analysis, calibration standards, instrument blanks and quality control standards were made such that they contained representative (appropriately diluted) amounts of each of the extraction solutions used (i.e. one for each of the reagents in SEDEX and an additional one for TP digestion). The appropriate, matrix-matched set of standards was then used when analyzing extractions in each of the solutions used.

Table A9-1 Summary of detection limits for parameters reported. Total number of samples for which parameter reported and number of samples below the detection limit are shown. The method used to determine the detection limit reported with results is summarized for each instrument used.

Instrument	Detection Limit Source	Method	Parameter	Detection Limit	Number of Non-detects
ICP-OES *Thermo Scientific iCAP 6300 Duo*	sd of lowest standard × students T × dilution factor	TP Extraction	TP	2.9 mgP kg^{-1}	0/115
			Na	99 mgNa kg^{-1}	0/115
			K	146 mgK kg^{-1}	0/115
			Ca	9.8 mgCa kg^{-1}	0/115
			Mn	1.9 mgCa kg^{-1}	0/115
			Fe	11.5 mgFe kg^{-1}	0/115
		SEDEX	P_{Ex}^{I}	0.619 mgP kg^{-1}	5/15
			P_{Hum}^{II}	0.619 mgP kg^{-1}	0/15
			P_{Fe}^{III}	0.619 mgP kg^{-1}	0/15
			P_{Ca}^{IV}	0.619 mgP kg^{-1}	0/15
			P_{Det}^{V}	0.619 mgP kg^{-1}	0/15
			P_{Org}^{VI}	0.619 mgP kg^{-1}	0/15
CHNS *Elementar vario EL cube*	Manufacturer Limitation	CHNS	TC	1% C	0/28
			OC	1% C	5/36
			TN	1% N	28/28
			ON	1% N	36/36